Workshop on 核磁共振方法研習會

" Recent Advances in Biomacromolecular NMR Spectroscopy"

Institute of Biomedical Sciences, Academia Sinica, Taipei, Taiwan

2011

Feb.17-18

Program Overview

Day 1 : February 17th, 2011 (Thursday)

Place : B1B Lecture Room

Lectures Sessions

08:30-09:00	Registration	
09:00-09:10	Opening Remark *by Dr. Tai-huang Huang*	
09:10-10:00	Lecture I - **NMR in an integrated drug discovery approach** *by Dr. Wolfgang Jahnke, Novartis Institutes for BioMedical Research, Switzerland*	1
10:00-10:50	Lecture II - **Recent Development of Paramagnetic Relaxation Enhancement (PRE) in Studying Protein Solution Dynamics**. *by Dr. Chun Tang, Chinese Academy of Sciences Wuhan, China*	2
10:50-11:10	Coffee Break	
11:10-12:00	Lecture III - **A small/wide-angle X-ray scattering instrument for structural studies of soft matter at the NSRRC** *by Dr. U-Ser Jeng, National Synchrotron Radiation Research Center, Taiwan*	3
12:00-14:00	Lunch Break	
14:00-18:00	HFNMRC Users Presentations & TMRS Activities	
	14:00-14:30 TMRS Annual Meeting	
	14:30-15:50 Session I : <u>Young Researcher Presentations (I)</u>	
	Applying diffusion MRI techniques to discover the white matter connectivity in human brain *Yu-Chun Lo (Prof. Wen-Yih Tseng Lab, NTU)*	4
	Supra-molecular Magnetic Nanoparticles for Contrast Enhancement in MR Molecular Imaging *Chaohsiung Hsu (Prof. Lian-Pin Hwang/Yung-Ya Lin Lab, NTU)*	5
	Comprehensive Solid-State NMR Study of Octacalcium Phosphate Incorporated with Succinate *Wen-Tin Tsai (Prof. Jerry C. C. Chan Lab, NTU)*	6
	Hydrogen bonding network in Nafion proton exchange membrane *Zhen Wu (Prof. Shangwu Ding Lab, NSYSU)*	7
	15:50-16:20 Coffee Break	

16:20-17:00 Session II : Young Researcher Presentations (II)

Characterization of a Novel Cysteine Protease Inhibitor, Crammer, from Drosophila melanogaster, and its Potential Role in Cathepsin Regulation 8
Tien-Sheng Tseng (Prof. Ping-Chiang Lyu Lab, NTHU)

Study on complex structure between human synaptotagmin I (syt I) C_2B domain and inositol hexakisphosphate (IP_6) by NMR 9
Meng-Che Chuang (Prof. Chin Yu Lab, NTHU)

17:00-18:00 Session III : Invited Young Scientist Talks

New Insights of 12-Tungstophosphoric Acid from Solid-state ^{31}P NMR of Absorbed Trimethylphosphine Oxide and Introduction of the New High-Field NMR Facilities at Instrumentation Center of National Taiwan University 10
Shing-Jong Huang, PH.D. (Department of Chemistry, NTU)

NMR and X-ray analysis of DNA recognition by Myb3 DNA binding domain from *Trichomonas vaginalis* 11
Yuan-Chao Lou, PH. D. (Institute of Biomedical Science, Academia Sinica)

Day 2 : February 18th, 2011 (Friday)

Place : B1A Meeting Room

Practical Sessions

08:30-09:00 Registration

09:00-10:30 Practical Session I-**Drug discovery by NMR** 12
by Dr. Wolfgang Jahnke, Novartis Institutes for BioMedical Research, Switzerland

10:30-10:50 Coffee Break

10:50-12:20 Practical Session II- **Paramagnetic Relaxation Enhancement (PRE)** 14
by Dr. Chun Tang, Chinese Academy of Sciences Wuhan, China

12:20-14:00 Lunch Break

14:00-15:30 Practical Session III- **SAXS Reveals Protein Structures** 26
by Dr. U-Ser Jeng & Dr. Yu-Shan Huang, National Synchrotron Radiation Research Center, Taiwan

15:30-15:50 Coffee Break

15:50-17:20 Practical Session IV: ***Discussion***

Lectures Sessions

NMR in an integrated drug discovery approach

Wolfgang Jahnke
Novartis Institute for Biomedical Research, Basel, Switzerland
wolfgang.jahnke@novartis.com

NMR is a useful and highly versatile biophysical technique that can support the drug discovery process in a variety of ways[1]. On one hand, biomolecular NMR is a very robust and reliable method to detect and characterize protein-ligand interactions. On the other hand, NMR can give structural information on proteins and protein-ligand complexes.

In my presentation, I will review the most commonly used NMR experiments to detect ligand binding, and I will present two recent applications of valuable NMR contributions to the drug discovery process: Allosteric non-bisphosophonate inhibitors of FPPS[2], and allosteric inhibitors of Abl kinase[3].

[1] W. Jahnke "Perspectives of biomolecular NMR in drug discovery: The blessing and curse of versatility" J. Biomol. NMR 39, 87-90 (2007)
[2] W. Jahnke, J.-M. Rondeau, S. Cotesta, A. Marzinzik, X. Pellé, M. Geiser, A. Strauss, M. Götte, F. Bitsch, R. Hemmig, C. Henry, S. Lehmann, J.F. Glickman, T.P. Roddy, S.J Stout, J. R. Green "Allosteric non-bisphosphonate FPPS inhibitors identified by fragment-based discovery" Nature Chemical Biology 6, 660-666 (2010)
[3] W. Jahnke, R.M. Grotzfeld, X. Pellé, A. Strauss, G. Fendrich, S.W. Cowan-Jacob, S. Cotesta, D. Fabbro, P. Furet, J. Mestan, A. Marzinzik "Binding or bending: Distinction of allosteric Abl kinase agonists from antagonists by an NMR-based conformational assay" J. Am. Chem. Soc. 132, 7043-7048 (2010)

Recent Development of Paramagnetic Relaxation Enhancement (PRE) in Studying Protein Solution Dynamics

Chun Tang
State Key Laboratory of Magnetic Resonance and Atomic Molecular Physics, Wuhan Institute of Physics and Mathematics, Chinese Academy of Sciences, Wuhan, Hubei 430017, China

Proteins in solution constantly undergo conformational fluctuations, thus to fulfill their specific functions. Most established NMR methods including relaxation dispersion afford only timescales of protein dynamics. Recently, we applied paramagnetic relaxation enhancement (PRE) technique to directly visualize structures of low-populated species in a dynamic system. The technique utilizes large dipole moment of an unpaired electron and $<r^{-6}>$ distance dependency of PRE effect. I will talk about applications of PRE to visualize protein-protein encounter complexes, protein domain movement, and protein oligomerization. In addition, ongoing work studying the dimerization of ubiquitin will also be presented.

To study protein dynamics using PRE, a paramagnetic probe is introduced at specific site, often through a surface cysteine residue. The flexible linker between the paramagnetic center and protein backbone results in uncertainty of the observation point. We have designed a rigid probe that permits detection of subtle movement. We have improved the PRE technique, called differential scaled PRE (DiSPRE); when using multiple probes of different paramagnetic strengths, we can extract both temporal and spatial characterization for an exchanging process. Taken together, paramagnetic NMR offers new opportunities to visualize protein structure and dynamics in solution.

A small/wide-angle X-ray scattering instrument for structural studies of soft matter at the NSRRC

U-Ser Jeng, Chiu-Hun, Su, Chun-Jen Su, Wei-Chung Chuang, Yu-Shan Huang
National Synchrotron Radiation Research Center, Taiwan

Research on soft matter with time-resolved small/wide-angle X-ray scattering (SAXS/WAXS) at NSRRC is blooming because of the much improved X-ray flux provided at the new SAXS beamline BL23A. The BL23A SWAXS endstation, open since May 2009, provides efficient collection of high-quality data that follow closely the standards of the world's leading SAXS instruments at ESRF, SOLEIL, APS or SPring-8 in static measurements of equilibrium morphology or slow kinetics in solutions and films. Presented in this talk are the features of the new BL23A SWAXS endstation, including simultaneous, time-resolved SAXS/WAXS with DSC, shear, a stretching device, and a stopped-flow device for structural kinetics of polymers, nanoparticles, liquid crystals and biomacromolecules in solution. SAXS/WAXS applications on biomacromolecular solutions or oriented films will be emphasized, including protein folding-unfolding and peptide-membrane binding. The future *X-ray photon correlation spectroscopy* (XPCS) beamline with the Taiwan Photon source (TPS), aiming for structural kinetics and dynamics of thermal equilibrium structures on a time scale from hundreds of seconds to milliseconds, will be briefed.

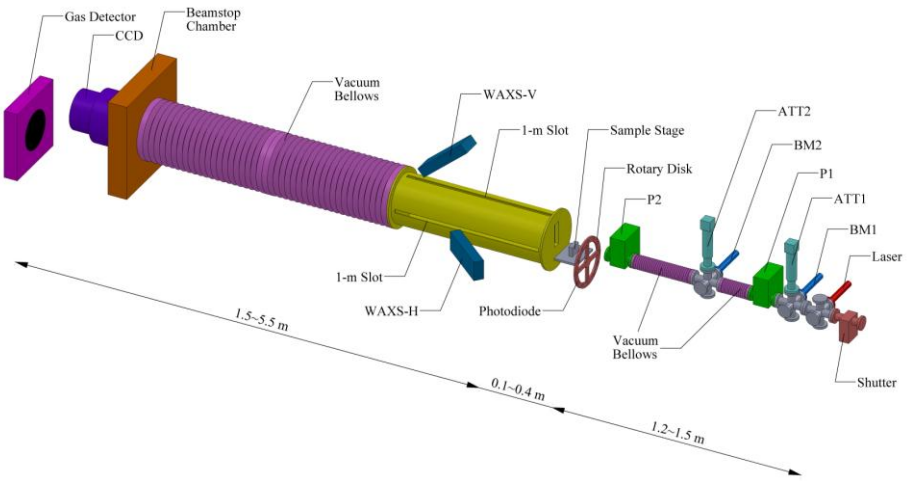

Figure 1 Schematic of the BL23A SAXS/WAXS instrument.

HFNMRC Users Presentations & TMRS Activities

Applying diffusion MRI techniques to discover the white matter connectivity in human brain

Yu-Chun Lo 羅伃君 and Wen-Yih Isaac Tseng
Institute of Biomedical Engineering, National Taiwan University

Neuroscience is an interdisciplinary science that collaborates with other fields. Neuroimaging is a part of neuroscience and includes the use of various techniques to either directly or indirectly image the structure, function, or pharmacology of the brain. Neuroimaging studies focus on discovering the primary and cognitive functions in the brain. Recently, magnetic resonance imaging (MRI) has become an important technique to discover the human brain non-invasively. Advances in MRI methodology, such as the functional MRI and the diffusion MRI, and related analytic strategies allow researchers to test the brain connectivity models related to healthy patterns and disease pathology in psychiatric disorders.

There are four main topics targeted to diffusion spectrum imaging (DSI) techniques for clinical applications in this dissertation. First, we introduced the diffusion MRI techniques and related analytic approaches, such as voxel based morphometry (VBM) and tractography-based morphometry. Second, we analyzed white matter tracts in the fronto-striato-thalamic circuitry of the healthy human brain using DSI data and found the gender and handedness factors should be considered when one evaluates the impairment of the fronto-striato-thalamic circuitry. Third, we aimed to further explore white matter abnormalities in patients with obsessive-compulsive disorder (OCD) in DSI and tractography of targeted white matter tracts in the fronto-striato-thalamic circuitry which most probably play an important role in OCD neuropathology. This study supports the white matter abnormalities of patients with OCD, which corroborates neurobiological models that posit a defect in fronto-striato-thalamic circuitry in OCD. Finally, we analyzed the microstructural integrity of the long-range connectivity related to social cognition and language processing with diffusion tractography among adolescents with autism compared to neurotypicals. The loss of leftward asymmetry and reduction of interhemispheric connection in adolescents with autism suggest alterations of the long-range connectivity involved in social cognition and language processing.

In summary, we successfully applied the DSI techniques to healthy participants and patients with mental disorders. The translation of DSI technique from laboratory to clinical setting is potentially feasible. Moreover, the clinical experience and technical strengths provide a strong basis for us to extend to imaging genetics, aiming to determine effective endophenotypes of psychiatric disorders. In the future, it is plausible that brain imaging may serve as effective endophenotypes that link clinical manifestation (phenotypes) and the biological variables (genotypes). The methodology of validating endophenotype will be readily extended to other psychiatric disorders.

Supra-molecular Magnetic Nanoparticles for Contrast Enhancement in MR Molecular Imaging

Chaohsiung Hsu 許朝雄 and Yung-Ya Lin
Taiwan International Graduate Program (TIGP), Academia Sinica (and National Tsing Hua University)

Comprehensive Solid-State NMR Study of Octacalcium Phosphate Incorporated with Succinate

Tim W. T. Tsai and Jerry C. C. Chan
Department of Chemistry, National Taiwan University

Octacalcium phosphate (OCP) is an important model compound in the study of biomineralization. The octacalcium phosphate incorporated with succinate (OCPS) is hypothesized as a component of mineral granules in mitochondria.[1] It is therefore *in vitro* prepared and characterized mainly by solid-state NMR spectroscopy. Accordingly, the molecular formula of OCPS is determined to be $Ca_{7.81}(HPO_4)_{1.82}(PO_4)_{3.61}(\text{succinate})_{0.56}\,zH_2O$, where $z \leq 0.5$. Furthermore, the succinate molecule is found to be in the hydration layer of OCPS. The stability of OCPS is significantly higher than OCP with respect to the hydrolysis reaction at high pH and/or high temperature conditions. We conclude that the hydration layer of OCP is playing the key role in the structural transformation of OCP.

References:

1 J. W. Greenawalt, C. S. Rossi and A. L. Lehninger, *J. Cell Biol.*, 1964, **23**, 21-38.
2 M. Markovic, B. O. Fowler and W. E. Brown, *Chem. Mater.*, 1993, **5**, 1401-1405.
3 T. W. T. Tsai, F. C. Chou, Y. H. Tseng and J. C. C. Chan, *Phys. Chem. Chem. Phys.*, 2010, **12**,

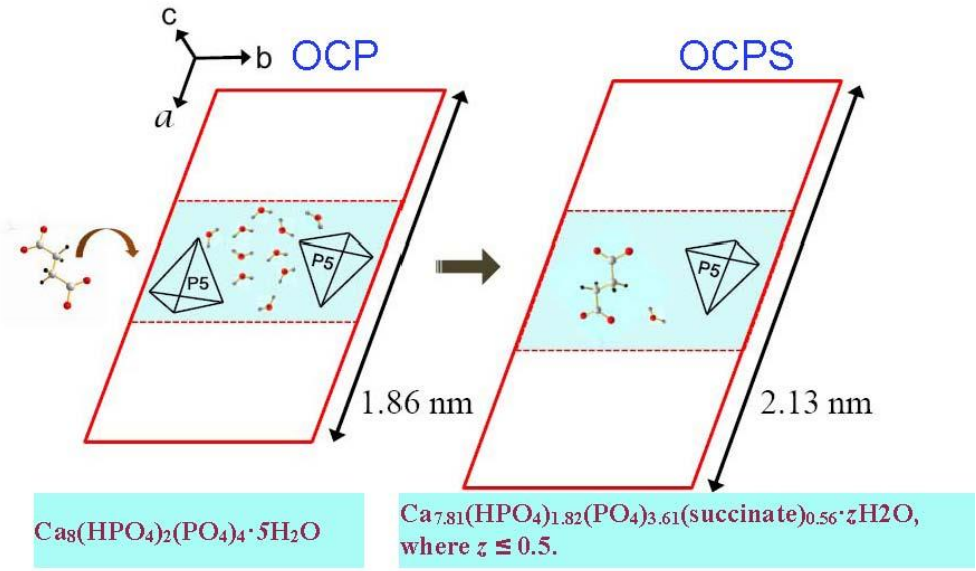

Hydrogen bonding network in Nafion proton exchange membrane

Zhen Wu 吳振 [1], Peter Chu[2] and Shangwu Ding[1]
[1]*Department of Chemistry, National Sun Yat-Sen University*
[2]*Department of Chemistry, National Central University*

The structural and dynamical properties of Nafion membranes swollen with water molecules in varied hydration level under proton and sodium forms have been investigated by NMR variable temperature experiments and pulse field gradient techniques. By analyzing the spin-lattice relaxation time of water in membranes as a function of temperature, the activation energy is obtained in light of BPP theory. In proton form of membranes, the activation energy is up to 43500 J · mol^{-1} for dehydrated state (λ=6) and down to 16500 J · mol^{-1} for fully hydrated state (λ=22), respectively. In sodium form of membranes, the activation energy is up to 35500 J · mol^{-1} for dehydrated state (λ=8) and down to 15500 J · mol^{-1} for fully hydrated state (λ=17), respectively. The *ab initio* calculations from triflic acid (CF_3SO_3H), CF_3SO_3Na and H_2O, as model system, are carried out in order to characterize the dependency of rotational correlation time and activation energy on hydrogen bonding network within Nafion membranes. With less water content, the results indicate that most of water molecules are involved in hydrogen bonding network close to the sulfonate acid groups which is contrary to the case of higher water content. These results are useful in understanding the behavior of dynamics and proton transfer for Nafion proton exchange membrane.

Characterization of a Novel Cysteine Protease Inhibitor, Crammer, from *Drosophila melanogaster*, and its Potential Role in Cathepsin Regulation

Chao-Sheng Cheng 曾天生, Tien-Sheng Tseng, Yu-Nan Liu, Dian-Jiun Chen, Ping-Chiang Lyu

Institute of Bioinformatics and Structural Biology, National Tsing Hua University

Drosophila melanogaster crammer belongs to a novel class of cysteine protease inhibitors and has been found to be involved in the formation of *Drosophila* long-term memory (LTM). The biophysical properties of crammer remain elusive. Here we found that the oligomeric state of crammer is pH-dependent. At neutral pH, *in vitro*, crammer exists as a disulfide bonded dimer, while at acidic pH, the monomer is predominant. However, *in vivo*, crammer likely exists as a monomer inside the lysosome. Our inhibitory assay shows that only monomeric crammer, but not a dimer, can act as a strong competitive inhibitor to suppress *Drosophila* cathepsin, which is distinct from the conclusions of previous studies. In particularly, Cys72 in crammer is not only responsible for the formation of intermolecular disulfide bond but also crucial for cathepsin inhibition. Finally, we also report the first structure of a propeptide-like inhibitor, crammer, and propose that monomeric crammer, like a molten globular protein, can undergo conformational change from the flexible state to the well-packed state upon binding with cathepsin. We presume the major driving forces for controlling structural change are the packing of aromatic residues and network salt bridges.

Study on complex structure between human synaptotagmin I (syt I) C_2B domain and inositol hexakisphosphate (IP_6) by NMR

Meng-Je Juang 莊孟哲 and Chin Yu
Department of Chemistry, National Tsing Hua University

Synaptotagmin I (Syt I) is a synaptic vesicle protein that contains two copies of highly conserved protein kinase C homology regions known as the C_2A and C_2B domains. The C_2A domain binds Ca^{2+} and the C_2B domain binds inositol polyphosphates (IP_4, IP_5, and IP_6). It has been reported that Ca^{2+} regulated exocytosis of secretory vesicles is proposed to be activated by Ca^{2+} binding to the C_2A domain and inhibited by inositol polyphosphate binding to the C_2B domain. Inositol hexakisphosphate (IP_6) is the principal storage form of phosphorus in many plant tissues. It has been shown that IP_6 is protective against Parkinson's disease *in vitro*. In the present study, we investigated the interaction of IP_6 with C_2B in the presence and absence of Ca^{2+} by various biophysical methods including isothermal titration calorimetry (ITC) and multidimensional NMR spectroscopy. These data show that IP6 binds specifically to the lysine-rich region of C_2B with similar binding strength both in the presence and absence of Ca^{2+}. The experimental data indicated IP_6 binding to C_2B is calcium independent. To understand the IP6 induced inhibition in exocytosis of secretory vesicles, we solved the solution structure of C2B-IP6 complex. This information will give clues to design better drugs for neurological disorders.

New Insights of 12-Tungstophosphoric Acid from Solid-state ^{31}P NMR of Absorbed Trimethylphosphine Oxide and Introduction of the New High-Field NMR Facilities at Instrumentation Center of National Taiwan University

Shing-Jong Huang 黃信炅
Department of Chemistry, National Taiwan University

The first part of this talk is intended to present our recent works (in collaboration with Prof. Shang-Bin Liu's group) on Keggin-type heteropolyacids such as 12-Tungstophosphoric acid ($H_3PW_{12}O_{40}$; HPW) using solid-state ^{31}P NMR of absorbed trimethylphosphine oxide (TMPO) probe molecule in conjunction with density functional theory (DFT) calculations. It will be shown that various protonated $TMPOH^+$ and $(TMPO)_2H^+$ adducts may be unambiguously identified using $^{31}P\{^1H\}$ Lee-Goldburg cross-polarization (LG-CP) HETCOR and ^{31}P-^{31}P DQ correlation techniques. Moreover, it was found that transport of TMPO absorbate in HPW adsorbent invokes a desorption/absorption process associated with the $(TMPO)_2H^+$ adducts. Consequently, three types of protonic acid sites with distinct superacidic strengths, corresponding to the observed ^{31}P chemical shifts of 92.1, 89.4, and 87.7 ppm, were identified for TMPO/HPW system. Together with the results from DFT calculations, thus, the $TMPOH^+$ complexes are most likely associated with protons located at three different terminal oxygen (O_d) sites of the $PW_{12}O_{40}^{3-}$ polyanions. Similar techniques have also been applied to other heteropolyacid systems, such as alkali ion-exchanged $Cs_xH_{3-x}PW_{12}O_{40}$ and $H_3PMo_{12}O_{40}$ (HPMo).

In the second part of this talk, I will briefly introduce the new high-filed NMR facilities at Instrumentation Center of National Taiwan University (NTU). This new 800 MHz NMR spectrometer (Bruker AVANCE III), which is located at the Chemistry Building of NTU, was installed just before the end of 2009. This spectrometer (under the supervision of Prof. Ying-Chih Lin) is also equipped with several probeheads for solution-state applications, including a 5 mm TCI cryoprobe, a 5 mm TXI, and a 5 mm BBO probes and also equipped with the solid-state accessories. We are also anticipating a new solid-state Bruker AVANCE III 600 MHz NMR spectrometer (supervised by Prof. Jerry Chun-Chung Chan) to arrive and to be installed in the same facility by mid-2011. With these state-of-the-art instruments, we hope to offer the best services to the NMR communities and to contribute to the NMR-related research in Taiwan.

NMR and X-ray analysis of DNA recognition by Myb3 DNA binding domain from *Trichomonas vaginalis*

Yuan-Chao Lou 羅元超, Shu-Yi Wei, Meng-Ru Ho, Jung-Hsiang Tai and Chinpan Chen
Institute of Biomedical Sciences, Academia Sinica

Trichomonas vaginalis, a protozoan parasite, is the causative agent of trichomoniasis, which is a common but often neglected sexually transmitted disease. The *ap65-1* gene of *T. vaginalis*, encoding a 65-kDa surface adhesion protein which is associated with the cytoadherence of *T. vaginalis* to the host cells, is regulated by Myb proteins through the Myb recognition elements (MREs). Among the identified Myb proteins (Myb 1 to 3), Myb3 interacts with the MRE-1 element. We identified that $Myb3_{53\text{-}180}$, containing two Myb-like DNA-binding motifs (designated as R2 and R3 motifs) and an extension of 31 residues at C-terminus (Ile^{150}-Lys^{180}), is the essential fragment for DNA recognition. And interestingly, the removal of C-terminal 31 residues reduces the DNA binding ability significantly. The structural basis of $Myb3_{53\text{-}180}$/DNA interaction was investigated by X-ray crystallography and showed that only the third helixes of both R2 and R3 motifs are responsible for DNA recognition. In the complex structure, the C-terminal 31 fragment forms a significant b-hairpin, but no direct interactions between DNA and the 31 residues can be observed. Using SPR, ITC and site-directed mutagenesis, we showed the importance of C-terminal fragment in DNA binding. Also, paramagnetic NMR was applied to investigate the interactions between $Myb3_{53\text{-}180}$ and DNA, and will be presented in detail in this talk.

Practical Sessions

Drug discovery by NMR

Dr. Wolfgang Jahnke

Drug discovery by NMR - Practical session

Wolfgang Jahnke

Workshop "Recent advances in biomacromolecular NMR spectroscopy"

18 February 2011

NOVARTIS

Agenda

- How to build a fragment library
  - Presentation and questions/answers
- How to analyze NMR fragment screening data
  - Practical session

Aspects of a fragment library

- Typically between 500 and 5000 compounds
  - Generally high hit rate
- Satisfy „rule of three" (Congreve et al. DrugDiscovToday 8,876, 2003)
  - MW < 300Da (typically < 250Da)
  - clogP < 3
  - # H-bond donors < 3, # H-bond acceptors < 3
- Satisfy diversity criteria
- Exclude reactive groups
- Fragments contain chemical handles for synthetic follow-up

Process of creating the library

- Solubilize candidate fragments in dmso-d_6
- Collect LC-MS data
  - Continue if purity >85% and mass OK
- Collect NMR spectra (in aqeous buffer)
  - Continue if structure is OK and solubility > 500uM: Fragment accepted
- Peak picking
- Design mixtures based on pick picked spectra
  - Minimize overlap between fragments
- Physically add the accepted fragments into the mixtures

Flowchart for NMR-based fragment screening

- Collect reference spectra of free mixtures without protein
  - [fragment] = 200uM
  - T1rho, waterLOGSY, STD
- Collect spectra of mixtures in the presence of target protein
  - [fragment] = 200uM, [target] = 5-10uM
- Compare spectra with and without protein, to obtain preliminary hit list
- Test all preliminary hits as single compounds with and without protein, to obtain final hit list
- If known high-affinity ligand is available, record competition spectra

Practical session

Analysis of three fragment screening mixtures against target X

- Which fragments bind to target X, and are they competitive with a known high-affinity inhibitor?

Practical session – how to proceed (1)

Analysis of three fragment screening mixtures against target X

- Using Topspin and spectra directory Jahnke, please process spectra
  - 110,111,112 – 1H, T1r, wL spectra of mixture 1 + targetX
  - 120,121,122 – 1H, T1r, wL spectra of mixture 2 + targetX
  - 130,131,132 – 1H, T1r, wL spectra of mixture 3 + targetX
  - 10,11,12 – 1H, T1r, wL spectra of free mixture 1
  - 20,21,22 – 1H, T1r, wL spectra of free mixture 2
  - 30,31,32 – 1H, T1r, wL spectra of free mixture 3
  - 210,211,212 – 1H, T1r, wL spectra of mixture 1 + targetX + competitor
  - 220,221,222 – 1H, T1r, wL spectra of mixture 2 + targetX + competitor
  - 230,231,232 – 1H, T1r, wL spectra of mixture 3 + targetX + competitor
- Processing commands:
  - „qsin;fp“ for 1H, waterLOGSY spectra (e.g. 110, 112)
  - „rser 1 – qsin – fp – wrp 1111“, „rser 3 – qsin – fp – wrp 1113“ for T1r spectra (111)
    - Then superimpose procnos 1113 and 1111 to see T1r effect

Practical session – how to proceed (2)

- Process spectra of mixtures in presence of targetX, compare to spectra of free mixtures. Decide which peaks show T1rho/waterLOGSY effects
- Deconvolute the mixtures into their components
  - Mix 1: 1501, 1509, 1521, 1599, 1775, 1788, 1792, 1828
  - Mix 2: 1503, 1506, 1525, 1531, 1640, 1643, 1798, 1862
  - Mix 3: 1504, 1507, 1524, 1533, 1560, 1804, 1846, 1874
- Superimpose spectra of individual compounds onto mixtures, to decide which fragment is a hit.
- Then analyze the competition experiments to see whether hits are competitive, non-competitive or synergistic

Paramagnetic Relaxation Enhancement (PRE)

Dr. Chun Tang

Outline

1. How to introduce a paramagnetic probe to otherwise diamagnetic protein?
2. How to measure ^1H Γ_2 PRE rates?
3. How to apply PRE restraints in Xplor-NIH?
4. How to account for the mobility of paramagnetic probe?
5. Xplor-NIH calculations
6. What happens when the exchange is not so fast?

Part 1

Conjugation method

- protein engineering (ATCUN, LBT)
- chemical cross-linking

Selection of conjugation site (Cys)

- periphery of the interface
- solvent exposed (charged)
- frequently mutated or modified
- does not perturb structure (RDC, functional assay)
- iso-electrical
- too mobile?
- cross-validation

Probes of choice

- Gd^{3+} (DTPA, CLaNP, LBT)
- Mn^{2+} (EDTA)
- spin radical (PROXYL, TEMPO)
- Cu^{2+} (EDTA, ATCUN)
  - isotropic *g*-tensor
  - stereo-isomer

Conjugation of a probe

- protein purification
- preparation of probe, metal loading
- desalting, conjugation
- desalting, further purification

Part 2

PRE measurement

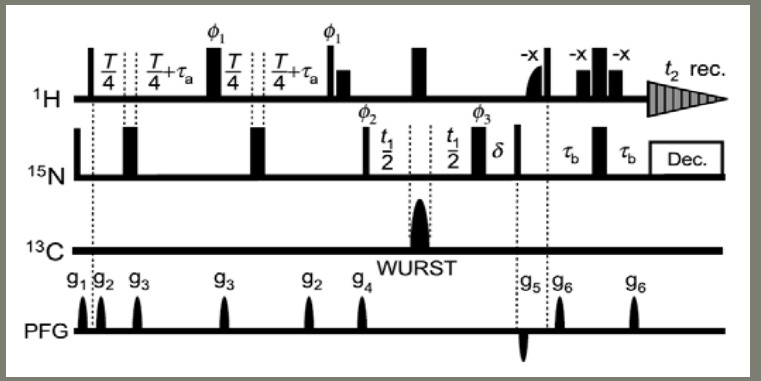


```
(p21 ph1):f3        ;
     5u             ;
     p17:gp13       ;
     95u            ;
1.5m

(p1 ph1):f1
     5u             ;
     p18:gp14       ;
     95u            ;
d13
(p22 ph6):f3
     5u             ;
     p18:gp15       ;
     95u            ;
d14
d13
(p1*2 ph2):f1
d13
     5u             ;
     p18:gp15       ;
     95u            ;
(p22 ph1):f3
d14
d13
     5u             ;
     p18:gp14       ;
     95u            ;
```

```
go=2 ph31 cpd3:f3
15m do:f3 wr #0 if #0 zd

15m id13
lo to 2 times 2
15m rd13

15m ip3
15m ip6
lo to 3 times 2

15m id0
15m ip31*2
lo to 4 times l1

exit
```

D13=5u, + in13, etc

D14=1/4J

$\Delta T = 4 \times in13$

Calculation of PRE

PRE $\Gamma_2 = R_2^{para} - R_2^{dia}$

$$\Gamma_2 = R_{2,para} - R_{2,dia} = \frac{1}{T_b - T_a} \ln \frac{I_{dia}(T_b) I_{para}(T_a)}{I_{dia}(T_a) I_{para}(T_b)}$$

$$\sigma(\Gamma_2) = \frac{1}{T_b - T_a} \times \sqrt{\frac{\sigma_{dia}}{I_{dia}(T_a)} + \frac{\sigma_{dia}}{I_{dia}(T_b)} + \frac{\sigma_{para}}{I_{para}(T_b)} + \frac{\sigma_{para}}{I_{dia}(T_b)}}$$

```
REMARK ROI 2D Peak Detection System, File: ./test.ft2
REMARK Detection Levels: -4.90275e+06 and 4.90275e+06
REMARK Detection: X(+/-1) Y(+/-1)
REMARK Interpolation: X(+/-1) Y(+/-1)
REMARK Position Tolerances: X(2.0) Y(2.0)
REMARK Sinc Detect ON, Height Adjustments: X(1.200) Y(1.000)
REMARK Sinc Detect Linewidths: X(15.0Hz) Y(0.0Hz)
REMARK Total Peaks: 89, Good Peaks: 89, Questionable Peaks: 0
REMARK Clusters: 87, Max Cluster Size: 2
REMARK ROI Spectral Axis Limits:

DATA  X_AXIS HN          1   664   10.803ppm    5.488ppm
DATA  Y_AXIS 15N         1   250  120.532ppm  107.950ppm

VARS   INDEX X_AXIS Y_AXIS DX DY X_PPM Y_PPM X_HZ Y_HZ XW YW XW_HZ YW_HZ X1 X3 Y1 Y3 HEIGHT DHEIGHT VOL PCHI2 TYPE ASS CLUSTID MEMCNT
FORMAT %5d %9.3f %9.3f %6.3f %6.3f %8.3f %8.3f %9.3f %9.3f %7.3f %7.3f %8.3f %8.3f %4d %4d %4d %4d %4e %4e %4e %.5f %d %s %4d %4d

    1   158.147     7.798  0.026  0.004    8.933  127.988  7147.996  10378.923    4.323    2.835    23.556   13.216  156  160    7    9 +2.884315e+07 +5.340616e+04 +1.457155e+08 0.00000 1 K6    1    1
    2    67.756     9.801  0.030  0.003    9.548  127.827  7640.587  10365.859    4.389    2.825    23.481   13.148   65   70    9   11 +2.863705e+07 +5.357532e+04 +1.531221e+08 0.00000 1 I13   2    1
    3    86.794    10.258  0.031  0.004    9.419  127.791  7536.841  10362.945    4.264    2.859    23.238   13.371   85   89   10   11 +1.889617e+07 +5.395776e+04 +1.168244e+08 0.00000 1 L67   3    1
    4   120.547    21.084  0.043  0.003    9.189  126.930  7352.899  10293.189    4.500    1.928    24.564   12.469  118  123   20   22 +2.161514e+07 +5.339950e+04 +1.596743e+08 0.00000 1 V98   4    1
    5   346.953    26.053  0.021  0.002    7.648  126.525  6119.632  10260.316    4.297    1.981    23.415   12.866  344  349   25   27 +2.464376e+07 +5.252870e+04 +1.813427e+08 0.00000 1 T9    5    1
    7   212.472    34.885  0.040  0.003    8.563  125.818  6851.950  10202.959    4.246    1.963    23.137   12.746  210  215   34   36 +2.162405e+07 +5.489718e+04 +1.535394e+08 0.00000 1 L58   7    1
   11   170.596    41.964  0.039  0.003    8.848  125.251  7080.156  10156.989    4.393    1.922    23.939   12.480  168  173   41   43 +2.112912e+07 +5.338405e+04 +1.522335e+08 0.00000 1 F46   11   1
   12   186.877    41.873  0.022  0.003    8.737  125.258  6991.432  10157.579    4.371    1.967    23.822   12.775  184  189   41   43 +2.328320e+07 +5.278652e+04 +1.688761e+08 0.00000 1 L15   12   1
   13   349.257    49.952  0.024  0.002    7.631  125.092  6106.529  10144.070    4.371    1.909    23.010   12.399  347  352   43   46 +2.569017e+07 +5.209529e+04 +1.709549e+08 0.00000 1 Q62   13   1
   16   383.019    49.149  0.012  0.002    7.946  124.676  6358.580  10110.330    3.680    2.020    19.660   13.115  381  385   48   50 +2.759611e+07 +5.379249e+04 +1.663983e+08 0.00000 1 D58   16   1
   17   245.277    50.300  0.014  0.002    8.339  124.584  6673.174  10102.056    3.717    2.008    20.250   13.587  243  248   49   51 +3.701639e+07 +5.557226e+04 +2.446576e+08 0.00000 1 L69   17   1
   18   174.391    50.693  0.045  0.005    8.822  124.552  7059.473  10100.300    4.492    2.118    24.482   13.703  172  177   50   51 +1.996311e+07 +5.477527e+04 +1.418876e+08 0.00000 1 L43   18   1
   19   249.827    54.040  0.020  0.003    8.314  124.219  6652.741  10073.319    4.225    1.994    23.024   12.952  247  251   54   56 +2.220866e+07 +5.294234e+04 +1.511594e+08 0.00000 1 L73   19   1
   20   436.031    56.093  0.015  0.002    7.040  124.120  5633.646  10065.232    3.930    1.940    21.416   12.652  434  438   55   57 +2.577211e+07 +5.319772e+04 +1.681299e+08 0.00000 1 S20   20   1
```


Setting of $\Delta T=T_b-T_a$

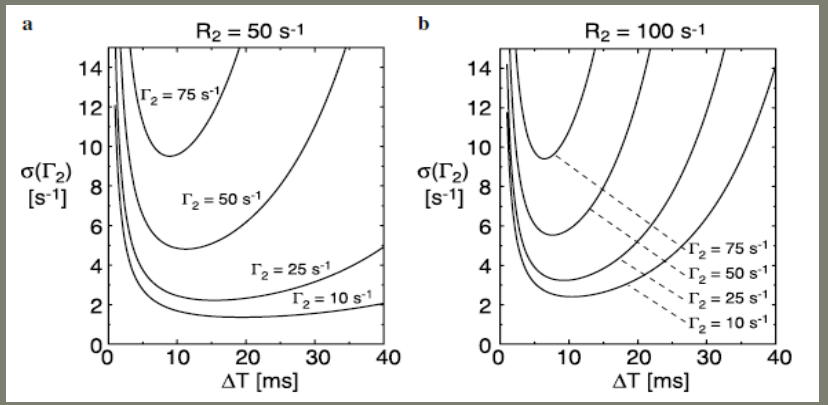

Single-time-point measurement of PRE

$$I_{\text{para}}(0) = I_{\text{dia}}(0)\frac{R_{2,\text{dia}}}{R_{2,\text{dia}}+\Gamma_2}\exp(-\Gamma_2\tau)$$

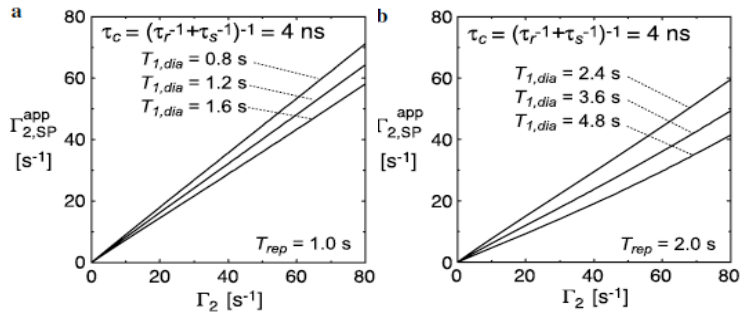

Complete longitudinal recovery is difficult

- > $5/R_1$ or > $5/(R_1+\Gamma_1)$
- > deuterated protein

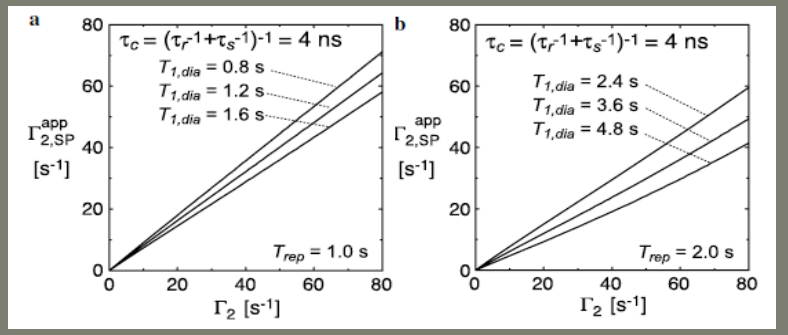

Part 3

Implementation of PRE restraints

$$E_{\text{Restraint}} = k \sum w_i (P^{obs} - P^{calc})^2$$

$$\Gamma_2 = \frac{1}{15}\left(\frac{\mu_0}{4\pi}\right)^2 \gamma_I^2 g^2 \mu_e^2 s(s+1)[4J(0) + 3J(\omega)]$$

PRE restraint format

```
assign (segid ALT* and resi 502 and name OP) (segid BLT0 and resid 321 and name HN) SUM 0.5000
assign (segid ALT* and resi 502 and name OP) (segid " " and resid 321 and name HN) 4.6 0.6 0.5000
assign (segid ALT* and resi 502 and name OP) (segid BLT0 and resid 322 and name HN) SUM 0.5000
assign (segid ALT* and resi 502 and name OP) (segid " " and resid 322 and name HN) 3.5 1.1 0.5000
assign (segid ALT* and resi 502 and name OP) (segid BLT0 and resid 323 and name HN) SUM 0.5000
assign (segid ALT* and resi 502 and name OP) (segid " " and resid 323 and name HN) 7.0 1.5 0.5000
assign (segid ALT* and resi 502 and name OP) (segid BLT0 and resid 324 and name HN) SUM 0.5000
assign (segid ALT* and resi 502 and name OP) (segid " " and resid 324 and name HN) 16.9 5.9 0.5000
assign (segid ALT* and resi 502 and name OP) (segid BLT0 and resid 326 and name HN) SUM 0.5000
assign (segid ALT* and resi 502 and name OP) (segid " " and resid 326 and name HN) 13.7 2.0 0.5000
assign (segid ALT* and resi 502 and name OP) (segid BLT0 and resid 327 and name HN) SUM 0.5000
assign (segid ALT* and resi 502 and name OP) (segid " " and resid 327 and name HN) 9.5 2.5 0.5000
assign (segid ALT* and resi 502 and name OP) (segid BLT0 and resid 328 and name HN) SUM 0.5000
assign (segid ALT* and resi 502 and name OP) (segid " " and resid 328 and name HN) 6.2 1.0 0.5000
```

- Ensemble representation
- sb mode and sbmf mode

$$\Gamma_2 = \frac{1}{15}\left(\frac{\mu_0}{4\pi}\right)^2 \gamma_I^2 g^2 \mu_e^2 S(S+1) < r^{-6} > \left\{ 4\tau_c + \frac{3\tau_c}{1 + (\omega_H \tau_c)^2} \right\}$$

```
for pre in (preSite1, preSite2, preSite3):
   pre.setTcType("fix")
   pre.setTauC( 12.8 )
   pre.setTiType("fix")
   pre.setTtType("fix")
   pre.setEquType("sb")
   pre.setSbmfType("taut")
   pre.setTauI(0.000)
   pre.setTauT(0.000)
   pre.setSclType("const")
   pre.setRlxType("r2dd")
   pre.setFreqI(600.14)
   pre.setSqn(0.5)
   pre.setGfac(0.4472)
   potList.append(pre)
   rampedParams.append( MultRamp(.01,10,"pre.setForce(VALUE)") )
   pass
```


equType - Type of back-calculation of PRE
"sb" : the SB equation (SB mode) [default]
"sbmf" : the SBMF equation (SBMF mode)

aveType - Type of averaging
"r-6" : averaging with <r^(-6)>
"r-3" : <r^(-3)>^2 (only for SB mode)

rlxType - Type of paramagnetic relaxation mechanism
"r2dd" : R2 relaxation enhancement by dipolar mechanism
"r2curie" : by Curie spin relaxation
"r2mix" : r2dd + r2curie
"r1dd" : R1 relaxation enhancement by dipolar mechanism
"r1curie" : by Curie spin relaxation
"r1mix" : r1dd + r1curie
For the SBMF mode, only r2dd and r1dd are supported.

funType - Type of penalty function
"square" : Squared well potential
"harmonic": Harmonic potential [default]
"onesixth": ((Gcal)^(-1/6)-(Gobs)^(-1/6))^2

http://nmr.cit.nih.gov/xplor-nih/doc/current/python/ref/prePot.html

sclType - Type of scaling
"const" : Constant scaling.
1.0 for all
"sigma" : Scaling based on error.
1.0/(error)^2
"obsig" : Scaling based on Gobs and error
Gobs/Gmax/(error)^2

tauc - correlation time (1/tc = 1/tr + 1/te)
taut - overall correlation time in the SBMF equation (1/tt=1/tc+1/ti)
freql - NMR frequency (MHz) [500.0]
gfac - electron g-factor [2.0]
sqn - electron spin quantum number [2.5]
gammal - nuclear gyromagnetic ratio [26.752196]

$$\tau_c = (\tau_r^{-1} + \tau_e^{-1})^{-1}$$

Part 4

Ensemble representation of paramagnetic probe

EDTA-Mn^{2+}

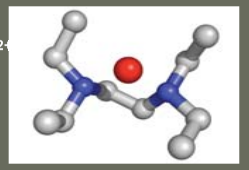

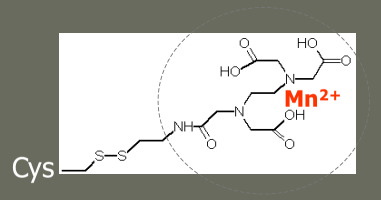

TEMPO

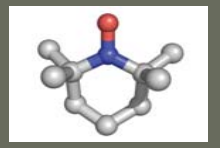

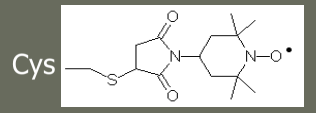

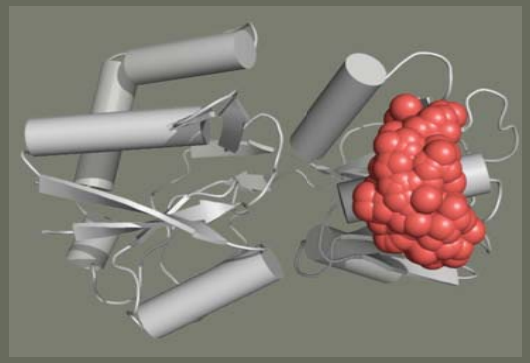

MTSL attached to a helix

XPlor-NIH: SB and SBMF mode

$$\Gamma_2 = S_{PRE}^2 < r^{-6} > f_{SB}(\tau_c) + (1 - S_{PRE}^2) < r^{-6} > f_{SB}(\tau_t)$$

$$S_{PRE}^2 \cong S_{PRE,angular}^2 S_{PRE,radial}^2$$

$$< r^{-6} >= \frac{1}{N} \sum^{N} r^{-6}$$

$$\frac{1}{\tau_t} = \frac{1}{\tau_c} + \frac{1}{\tau_i}$$

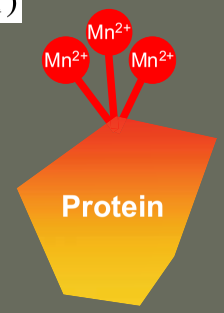

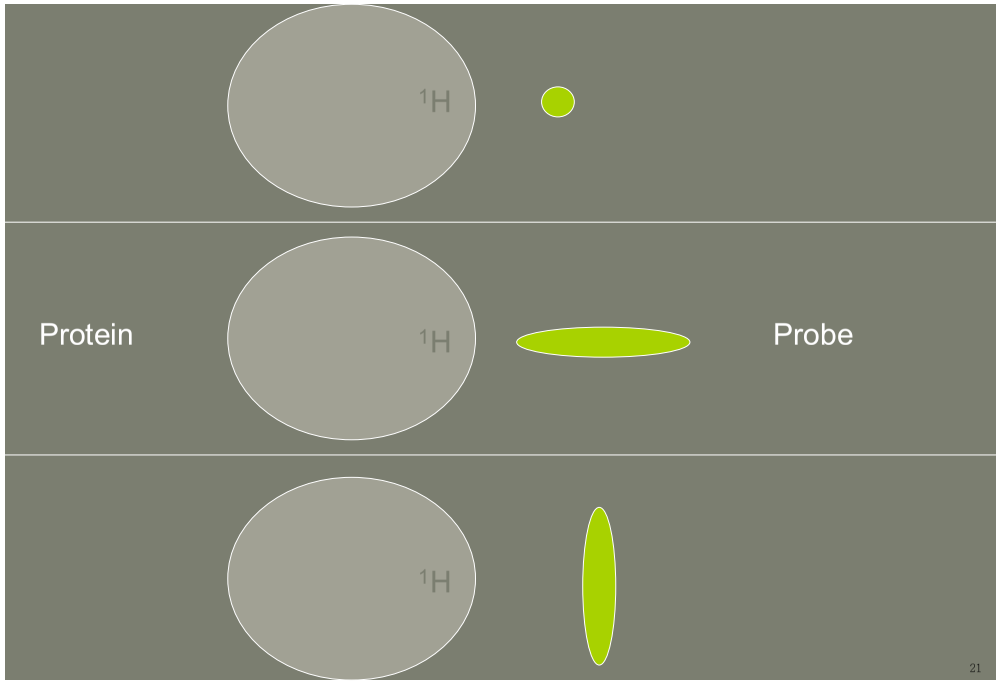

21

Part 5

Xplor-NIH

- Xplor 3.851
- CNS
- CYANA
- python interface

22

Invoke Xplor

% xplor -py

% pyXplor

% xplor

XPLOR>python

- command line input
- script based

xplor.command('struct @1gb1.psf')

23

Flow scheme

- PDB (mutant), PSF
- Topology, parameter file

- build hydrogen
- patch thiol linkage

- duplicate
- randomize the paramagnetic probe
- refine against PRE

$xplor_installation/eginput/pre/

24

```
PSF

       2 !NTITLE
 REMARKS FILENAME="../Psf/totalPlus3Alt.psf"
 REMARKS DATE:21-Aug-03  15:13:32       created by user: tangc

    3103 !NATOM
       1       1    MET  N    NH3   -0.100000       14.0070           0
       2       1    MET  HT1  HC     0.260000       1.00800           0
       3       1    MET  HT2  HC     0.260000       1.00800           0
       4       1    MET  HT3  HC     0.260000       1.00800           0
       5       1    MET  CA   CT     0.220000       12.0110           0
       6       1    MET  HA   HA     0.100000       1.00800           0
       7       1    MET  CB   CT    -0.200000       12.0110           0



     3246 !NBOND: bonds
          1       5       5       6       5       7       7       8
          7       9       7      10      10      11      10      12
         10      13      13      14      14      15      14      16
         14      17       5      18      18      19       2       1
          3       1       4       1      20      21      20      22
         22      23      22      24      24      25      24      26
         24      27      27      28      27      29      27      30
         30      31      30      32      32      33      32      34
         22      35      35      36      18      20      37      38
```


Standard topology and parameter files

$xplor_installation/toppar/

```
! BONDS

bonds      H    NA              $kbon      0.98
bonds      H    NB              $kbon      0.98
bond       H    NH2             $kbon      0.98
bond       H    NH1             $kbon      0.98
bond       H    OH              $kbon      0.96
bond       H    S               $kbon      0.96
```


PDB file of MTSL conjugate

```
ATOM      1  CA  MTS    79      -0.527  -0.793  99.449  1.00 20.00           C
ATOM      2  N01 MTS    79       0.353   0.222 101.367  1.00 20.00           N
ATOM      3  O01 MTS    79       1.044   0.878 102.147  1.00 20.00           O
ATOM      4  SG  MTS    79       0.128  -2.683  97.596  1.00 20.00           S
ATOM      5  C02 MTS    79      -1.306  -1.146 100.479  1.00 20.00           C
ATOM      6  C03 MTS    79      -0.852  -0.586 101.782  1.00 20.00           C
ATOM      7  C04 MTS    79       1.991  -0.473  99.683  1.00 20.00           C
ATOM      8  C05 MTS    79       0.594   0.115  99.871  1.00 20.00           C
ATOM      9  C06 MTS    79       0.480   1.529  99.300  1.00 20.00           C
ATOM     10  C07 MTS    79      -0.388  -1.665 102.754  1.00 20.00           C
ATOM     11  C08 MTS    79      -1.872   0.366 102.397  1.00 20.00           C
ATOM     12  CB  MTS    79      -0.764  -1.167  98.022  1.00 20.00           C
ATOM     13  H01 MTS    79      -2.184  -1.773 100.394  1.00 20.00           H
ATOM     14  HB1 MTS    79      -0.462  -0.365  97.343  1.00 20.00           H
ATOM     15  H03 MTS    79       2.077  -1.471 100.131  1.00 20.00           H
ATOM     16  H04 MTS    79       2.758   0.157 100.147  1.00 20.00           H
ATOM     17  H05 MTS    79       2.243  -0.559  98.620  1.00 20.00           H
ATOM     18  H06 MTS    79       1.214   2.206  99.752  1.00 20.00           H
ATOM     19  H07 MTS    79      -0.513   1.961  99.479  1.00 20.00           H
ATOM     20  H08 MTS    79       0.654   1.535  98.219  1.00 20.00           H
ATOM     21  H09 MTS    79       0.388  -2.304 102.315  1.00 20.00           H
ATOM     22  H10 MTS    79      -1.481   0.840 103.305  1.00 20.00           H
ATOM     23  H11 MTS    79      -1.223  -2.312 103.047  1.00 20.00           H
ATOM     24  H12 MTS    79       0.030  -1.229 103.668  1.00 20.00           H
ATOM     25  H13 MTS    79      -2.790  -0.166 102.669  1.00 20.00           H
ATOM     26  H14 MTS    79      -2.149   1.171 101.704  1.00 20.00           H
ATOM     27  HB2 MTS    79      -1.831  -1.346  97.848  1.00 20.00           H
ATOM     28  HG  MTS    79      -0.421  -3.450  98.549  1.00 20.00           H
```


Generate topology/parameter for paramagnetic probe

http://xray.bmc.uu.se/hicup/xdict.html

Topology file example
Parameter file example

Generate psf file from pdb file

```
rtf @../topallhdg_new.pro
end

parameter @../parallhdg_new.pro
end

segment
  name=" "
  SETUP=TRUE
  chain
    @../toph11.pep

coor @../1xyz.pdb
end
end

!delete select (resi 3) end

write psf output=1xyz.psf end

stop
```


Generate psf file for non-peptide

```
rtf @./topallhdg_new.pro end
rtf @./MTSL.top end

parameter @./parallhdg_new.pro end
parameter @./MTSL.par end

segment
   name=" "
   SETUP=TRUE
   chain
!      @../toph11.pep

coor @MTSL.pdb
end
end

write psf output=MTSL.psf end

stop
```

Example of the psf file

Build hydrogen atoms

```
hbuild select=(name H*) phistep=360 end

flags exclude * include bonds angle impr end

constraint fix (not name H*) end

mini powell nstep 1000 end
```



```
parameter @parallhdg_new.pro @PXD1.par end

structure @Acys.psf @PXD_2.psf @PXD_3.psf @PXD_4.psf @PXD_5.psf end
delete select (resn cys and name hg ) end
coor @Random1/temp1.pdb end
coor @Random1/temp2.pdb end
coor @Random1/temp3.pdb end
coor @Random1/temp4.pdb end
coor @Random1/temp5.pdb end

topology
  autogenerate angles=true end
  presidue ES
     group
     modify atom 1SG end
     group
     modify atom 2CD end
     add bond 1SG 2CD
     add angle 1CB 1SG 2CD
     add angle 1SG 2CD 2CE
     add dihedral 1CA 1CB 1SG 2CD
     add dihedral 1CB 1SG 2CD 2CE
  end
end

patch ES
  reference=1=(resi 112) reference=2=(resi 502)
end

write psf output=para_E.psf end
write coor output=para_E.pdb end

stop
```

Patch thiol linkage

Various energy functions in Xplor-NIH

noePot - NOE distance restraints
rdcPot - dipolar coupling
csaPot - Chemical Shift Anisotropy
cstMagPot - regne against chemical shift tensor magnitudes and orientations
jCoupPot - 3J-coupling
prePot - Paramagnetic relaxation enhancement
gyrPot - pseudopotential enforcing correct protein density
diffPot - refine against rotational diffusion tensor
residueAffPot - contact potential for hydrophobic attraction/repulsion
planeDistPot - distance between atoms and plane
xplorPot - use XPLOR potential terms
solnScatPot - potential for solution X-ray and neutron scattering
posSymmPot - restrain atomic positions relative to those in a similar structure
sardcPot - RDCs in steric alignment media

Skeleton of a typical script

```
import protocol
protocol.loadPDB("model.pdb")     #initialize coordinates

coolParams=[] # a list which specifies potential smoothing
# set up potential terms from NMR experiments, covalent geometry,
# and knowledge-based terms

# initialize coolParams for annealing protocol for each energy term

from ivm import IVM   #configure which degrees of freedom to optimize
dyn = IVM()

from simulationTools import AnnealIVM
coolLoop=AnnealIVM(dyn,...)      #create simulated annealing object, specify temperature schedule

def calcOneStructure( structData ):
    """ a function to calculate a single structure """
    # [ randomize velocities ]
    # [ perform high temp dynamics ]
    dyn.run()
    # [ cooling loop ]
    coolLoop.run()
    # [ final minimization ]
    dyn.run()
    structData.writeStructure(potList)  #write out pdb record to file
                                        # with energies, rmsd's in headers
                                        # a separate .viols file also written

from simulationTools import StructureLoop
StructureLoop(numStructures=100,                    #calculate all structures
              pdbTemplate='SCRIPT_STRUCTURE.sa',    #  in parallel, if desired
              structLoopAction=calcOneStructure).run() #also report stats at end
```


Duplicate paramagnetic probe

```
parameter @parallhdg_new.pro end

structure @xyz_3atcun.psf end

coor @./Random/startup4_13.pdb

vector do (segid "ALT0")
(name cu or ((resi 48 or resi 63) and (name cb or name hb* or name sg)))

for $an in (1 2 3 4 5 6 7 8 9) loop alts

evaluate ($al = "ALT" + encode($an) )

duplicate
   segid  = $al
   select = ( segid "ALT0" )
end

end loop alts

write psf output=xyz_3atcun10.psf end
write coor output=xyz_3atcun10.pdb end

stop
```


Randomize paramagnetic probe

Sample script: randomize.py

Multiple conformer/ensemble representation

Two tiers and two timescale

$$\Gamma_2^{calc}(i) = (1-\lambda)\Gamma_2^{specific}(i) + \lambda \sum_{j=1}^{N} \Gamma_2^{non-specific}(i,j)/N$$

stereospecific complex
(population 1-λ)

Encounter complex
(population λ)

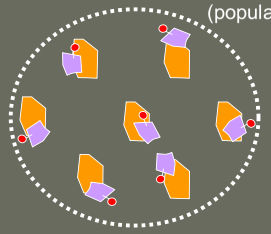

N HPr conformers by fixing EIN coordinates

Duplicate and randomize an entire protein or a portion of a protein

Sample script: randomize_init.inp

Implementing PRE restraints

```
assign (segid ALT* and resi 502 and name OP) (segid BLT0 and resid 321 and name HN) SUM 0.5000
assign (segid ALT* and resi 502 and name OP) (segid " " and resid 321 and name HN) 4.6 0.6 0.5000
assign (segid ALT* and resi 502 and name OP) (segid BLT0 and resid 322 and name HN) SUM 0.5000
assign (segid ALT* and resi 502 and name OP) (segid " " and resid 322 and name HN) 3.5 1.1 0.5000
assign (segid ALT* and resi 502 and name OP) (segid BLT0 and resid 323 and name HN) SUM 0.5000
assign (segid ALT* and resi 502 and name OP) (segid " " and resid 323 and name HN) 7.0 1.5 0.5000
assign (segid ALT* and resi 502 and name OP) (segid BLT0 and resid 324 and name HN) SUM 0.5000
assign (segid ALT* and resi 502 and name OP) (segid " " and resid 324 and name HN) 16.9 5.9 0.5000
assign (segid ALT* and resi 502 and name OP) (segid BLT0 and resid 326 and name HN) SUM 0.5000
assign (segid ALT* and resi 502 and name OP) (segid " " and resid 326 and name HN) 13.7 2.0 0.5000
assign (segid ALT* and resi 502 and name OP) (segid BLT0 and resid 327 and name HN) SUM 0.5000
assign (segid ALT* and resi 502 and name OP) (segid " " and resid 327 and name HN) 9.5 2.5 0.5000
assign (segid ALT* and resi 502 and name OP) (segid BLT0 and resid 328 and name HN) SUM 0.5000
assign (segid ALT* and resi 502 and name OP) (segid " " and resid 328 and name HN) 6.2 1.0 0.5000
```

```
   ensInterconvert - how to treat averaging over EnsembleSimulation members-
                     for SBMF mode. [Default: fast]
                  "fast"   : include average over EnsembleSimulation members in
                             calculation of order parameters and distance ave.
                  "slow"   : for each EnsembleSimulation member, calculate the
                             averages over ensemble of tags, and then perform
                             a linear EnsembleSimulation-weighted sum to compute
                             Gamma.
```


Ensemble structure refinement against PRE

Sample script: optimize.py

Evaluate the agreement between observed and calculated

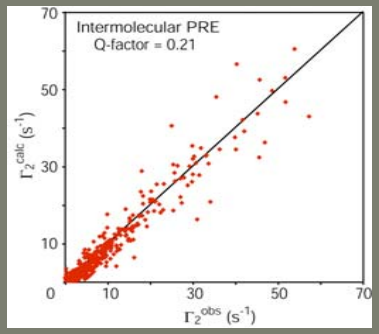

$$Q = \sqrt{\frac{\sum_i \left\{\Gamma_2^{obs}(i) - \Gamma_2^{cal}(i)\right\}^2}{\sum_i \Gamma_2^{obs}(i)^2}}$$

$$Q_e = \sqrt{\frac{\sum_i \left\{\Gamma_2^{obs}(i) - \left\langle\Gamma_2^{cal}(i)\right\rangle\right\}^2}{\sum_i \Gamma_2^{obs}(i)^2}}$$

41

Cross-validation of PRE restraints

- perturbation due to mutation / conjugation
- a random subset of PRE restraints
- data sets for each conjugation sites

42

Qualitative application of PRE (single structure)

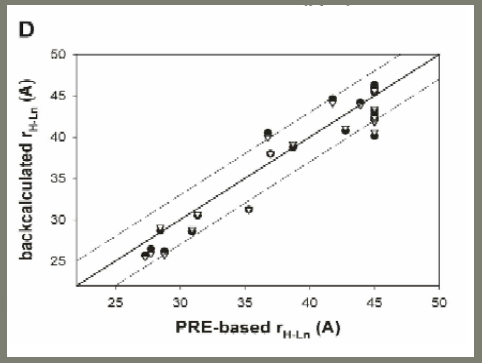

Ubbink et al *Biochemistry* 2008

43

Part 6

Intermediate exchange time-scale (upper μs to lower ms)

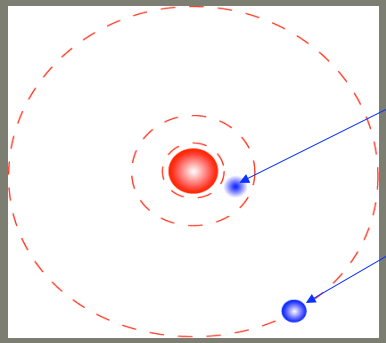

8Å
$\Gamma_{2,B}$=5600s^{-1}
p_B=1%

34Å
$\Gamma_{2,A}$=2s^{-1}
p_A=99%

$\Gamma_{2,obs}=\Gamma_{2,A}$x0.99+ $\Gamma_{2,B}$x0.01=58 s^{-1}

44

Simulating McConnell equation

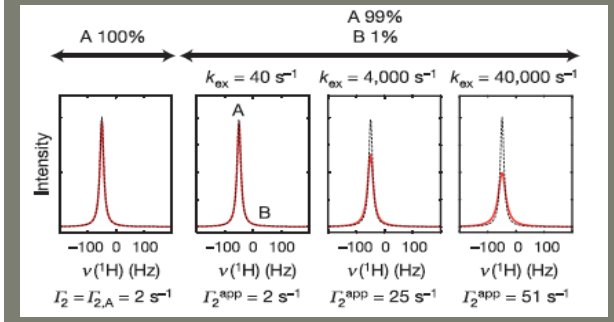

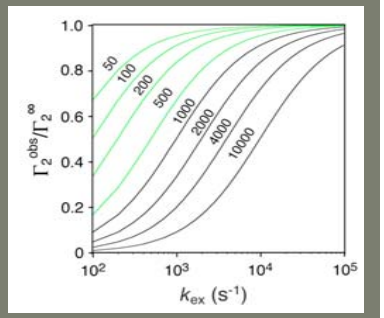

DiSPRE

45

Structure of protein by SAXS

Dr. Yu-Shan Huang

National Synchrotron Radiation Research Center

SAXS Reveals Protein Structures

Huang, Yu-Shan
NSRRC, Taiwan

Methods for 3D Structures of Biomolecules

- Nuclear Magnetic Resonance Spectroscopy
  - Atomic resolution
  - Difficulties in large protein studies
  - Excellence for dynamic studies
- Small-Angle X-ray Scattering
  - Resolution up to 1 nm
  - Excellence for functional solution structures, dynamic studies, and large proteins
- Macromolecule Crystallograhpy
  - Atomic resolution
  - Bottleneck for having a crystal
  - Difficulties in dynamic studies
- Cryo-Electron Microscopy
  - Resolution up to 1 nm
  - Excellence for large proteins

Small-Angle X-ray Scattering

SAXS is capable of revealing the aperiodic system, e.g. protein solutions. The protein particles in solutions are

•embedded with arbitrary orientation and with irregurlar distances in a matrix,

•limited in size, non-oriented, and aperiodic,

•assumed to be identical.

Solution structures can be probed by SAXS.

•For diluted monodisperse systems, SAXS can determine size (1 ~ 100 nm), shape, and the internal structure.

•For diluted polydisperse systems, SAXS can evaluate a size distribution under the assumption of a certain shape of the particles.

•For semi-dilute systems, the scattering curve is the product of the particle scattering function and of the interparticle interference function.

Books on SAS

- ***Small-Angle X-ray Scattering***, O. Glatter and O. Kratky (1982), Academic Press, http://physchem.kfunigraz.ac.at/sm/Software.htm
- ***Structure Analysis by Small Angle X-ray and Neutron Scattering,*** L.A. Feigin and D.I. Svergun (1987), Plenum Press, http://www.embl-hamburg.de/ExternalInfo/Research/Sax/reprints/feigin_svergun_1987.pdf
- ***Neutrons, X-Rays and Light, Scattering methods applied to soft condensed matter,*** P. Lindner and T. Zemb Eds, (2002) Elsevier, North-Holland

Reviews on SAS

- **Small angle scattering: a view on the properties, structures and structural changes of biological macromolecules in solution,** *Michel H. J. Koch, Patrice Vachette and Dmitri I. Svergun, Quarterly Review of Biophysics (2003), 36, 147-227.*
- **X-ray solution scattering (SAXS) combined with crystallography and computation: defining accurate macromolecular structures, conformations and assemblies in solution**, *Christopher Putnam, Michal Hammel, Greg Hura and John Tainer, Quarterly Review of Biophysics (2007), 40, 191-285.*
- **Analysis of X-ray and neutron scattering from biomacromolecular solutions**, *Maxim V. Petoukhov and Dmitri I. Svergun, Current Opinion in Structural Biology (2007), 17, 562-71.*

SAXS and NMR

Biophysical Journal Volume 83 August 2002 1127–1180

Quaternary Structure Built from Subunits Combining NMR and Small-Angle X-Ray Scattering Data

Maija-Liisa Mattinen,* Kimmo Pääkkönen,* Teemu Ikonen,† Jeremy Craven,‡ Torbjörn Drakenberg,* Riitta Serimaa,† Jonathan Waltho,‡ and Arto Annila*

Refinement of Multidomain Protein Structures by Combination of Solution Small-Angle X-ray Scattering and NMR Data

Alexander Grishaev,*,† Justin Wu,‡ Jill Trewhella,§ and Ad Bax*,†

Eur Biophys J (2006) 35: 313–327
DOI 10.1007/s00249-005-0037-3

Frank Gabel · Bernd Simon · Michael Sattler

A target function for quaternary structural refinement from small angle scattering and NMR orientational restraints

J Biomol NMR (2008) 41:199–208
DOI 10.1007/s10858-008-9258-y

A structure refinement protocol combining NMR residual dipolar couplings and small angle scattering restraints

F. Gabel · B. Simon · M. Nilges · M. Petoukhov · D. Svergun · M. Sattler

Eur Biophys J (2007) 37:95–104
DOI 10.1007/s00249-007-0170-2

A simple genetic algorithm for the optimization of multidomain protein homology models driven by NMR residual dipolar coupling and small angle *X*-ray scattering data

Fabien Marcoil · Christina Sizun · Javier Perez · Marc Schoenauer · Jean-Yves Lallemand · François Bontems

EM wave interacts with materials

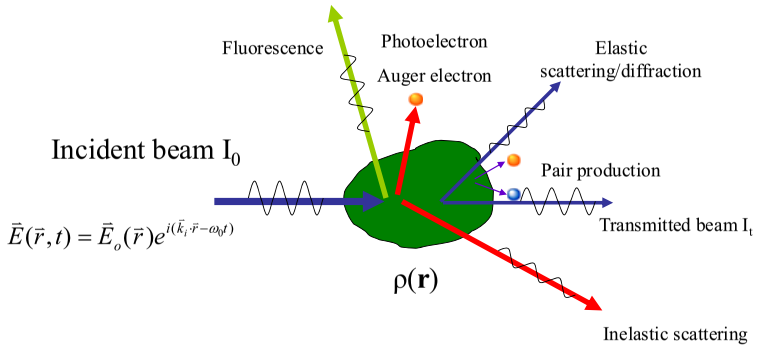

$$I_t(\lambda) = I_0 \exp(-\mu_\lambda t)$$

$$\mu_\lambda = \frac{1}{V_c}\sum_{n=1}^{N_n}\sigma_n \qquad \sigma_{tot} = \sigma_{pe} + \sigma_{el} + \sigma_{inel} + \sigma_{pp} + \ldots$$

Elastic (Thomson-Rayleigh) scattering: one electron

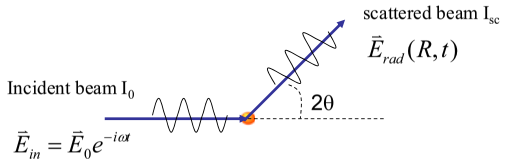

Classical dipole approximation

$$E_{rad}(R,t) = -E_{in} r_e \frac{e^{ikR}}{R}\cos 2\theta \qquad r_e \equiv \frac{e^2}{4\pi\varepsilon_0 mc^2} = 2.82\times10^{-5}\ \text{Å} \qquad \frac{I_{sc}}{I_0} = \frac{|E_{rad}|^2 R^2 \Delta\Omega}{|E_{in}|^2 A_0}$$

Differential cross-section

$$\frac{d\sigma}{d\Omega} \equiv \frac{I_{sc}}{(I_0/A_0)\Delta\Omega} = r_e^2\cos^2 2\theta = r_e^2 p \qquad \sigma_{tot} = \frac{8\pi}{3} r_0^2 = 0.665 barn$$

where p is 1, $\cos^2 2\theta$, or $(1+\cos^2 2\theta)/2$ for vertical, horizontal scattering planes of a horizontally polarized source, or unpolarized source, respectively.

Elastic scattering: atom and molecule

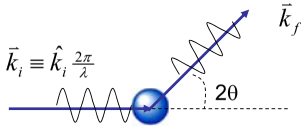

$$|\vec{Q}| \equiv |\vec{k}_f - \vec{k}_i| = 4\pi \sin\theta / \lambda$$

Total scattering length of one atom $-r_e f(\vec{Q}) = -r_e \int \rho(\vec{r}) e^{i\vec{Q}\cdot\vec{r}} dV$

Atomic form factor $f(Q,\lambda) \equiv f^0(Q) + f'(\lambda) + if''(\lambda)$

$$\sigma_{el} = \pi r_e^2 \int_{-1}^{1} (1+\cos^2 2\theta) f^2(Q,Z) d(\cos 2\theta)$$

Total scattering length of one molecule

$$-r_e F_{mol}(\vec{Q},\lambda) = -r_e \sum_{r_j} f_j(Q,\lambda) e^{i\vec{Q}\cdot\vec{r}_j}$$

Atomic form factor

$$f(Q,\lambda) = f^0(Q) + f'(\lambda) + if''(\lambda)$$

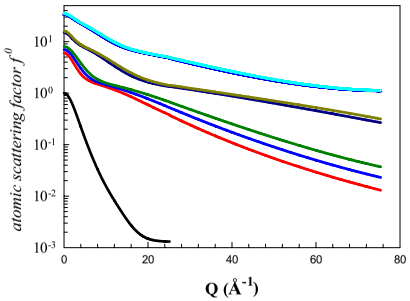

$$f^0(Q) = \sum_{i=1}^{4} a_i \exp[-b_i (Q/4\pi)^2] + c, \quad 0 < Q \equiv 4\pi \sin\theta/\lambda < 8\pi$$

$$\ln(f^0(Q)) = \sum_{i=0}^{3} a_i (Q/4\pi)^i, \quad 8\pi < Q \equiv 4\pi \sin\theta/\lambda < 24\pi$$

Based on relativistic Hartree-Fock calculations in IUCr Int'l table vol. C 6.1.

SAXS: elastic scattering

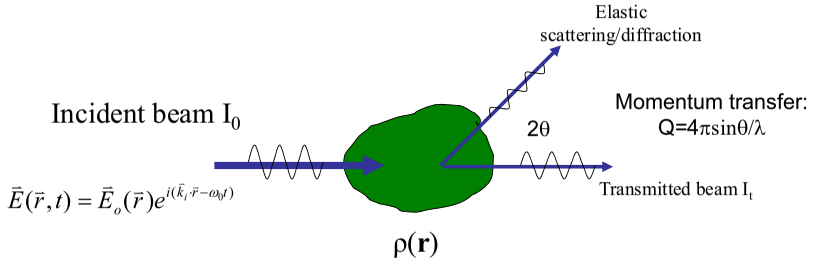

Small-Angle X-ray Scattering

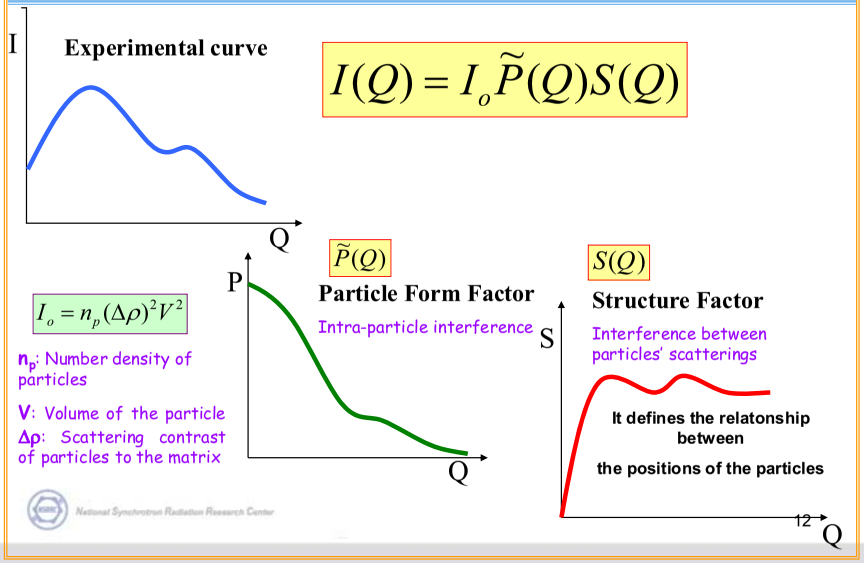

Sample requirements: Ideality and Monodispersity

Ideality:

- No intermolecular interaction at infinite dilution
- SAXS pattern is independent of concentration
- AUC, DLS

Monodispersity:

- Identical particles
- Purification protocol
- Mass Spec., AUC, DLS

SAXS Distinguishes Shapes and Sizes

- Sphere

$$\tilde{P}(Q) = \left(3j_1(QR)/QR\right)^2$$

- Ellipsoid

$$\tilde{P}(Q) = \int_0^1 \left|\frac{3j_1(v)}{v}\right|^2 d\mu$$

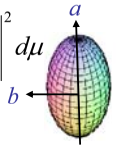

- Rod or disk

$$\tilde{P}(Q) = \int_0^1 \left|\frac{2J_1(v)}{v}\frac{\sin(w)}{w}\right|^2 d\mu$$

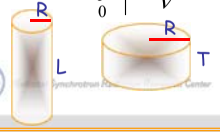

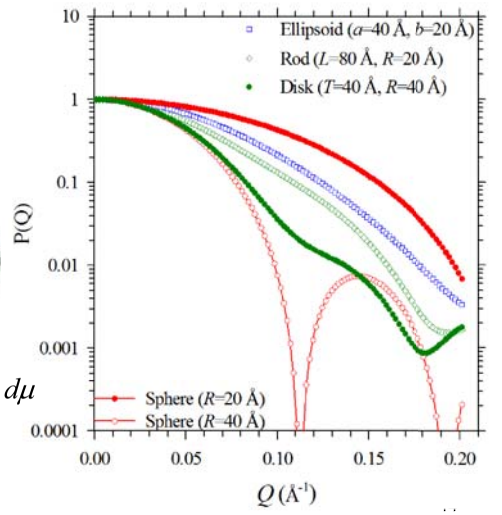

Small-Angle X-ray Scattering

For SAXS measurement, inelastic scattering is a smaller effect than elastic scattering. It only contributes to the background and does not yield any structural information.

$$-r_e f(\vec{Q}) = -r_e \int \rho(\vec{r}) e^{i\vec{Q}\cdot\vec{r}} dV$$

If the scatterers take all orientations.

$$f(Q) = 4\pi \int_0^\infty \rho(r) \frac{\sin Qr}{Qr} r^2 dr \qquad \left\langle e^{i\vec{Q}\cdot\vec{r}} \right\rangle_\Omega = \frac{\sin Qr}{Qr}$$

$$f(0) = 4\pi \int_0^\infty \rho(r) r^2 dr = Z$$

Debye formula (1915) $$I(Q) = \sum_{i=1}^{N}\sum_{j=1}^{N} f_i(Q) f_j(Q) \frac{\sin Qr_{ij}}{Qr_{ij}}$$

Small-Angle X-ray Scattering

$$A(\vec{Q})\cdot A^*(\vec{Q}) = \int\int \rho(\vec{r}_1)\rho(\vec{r}_2) e^{-i\vec{Q}\cdot(\vec{r}_1-\vec{r}_2)} dV_1 dV_2 \qquad A(\vec{Q}) = \int \rho(\vec{r}) e^{i\vec{Q}\cdot\vec{r}} dV$$

$$= \int\int \rho(\vec{r}_1)\rho(\vec{r}_1-\vec{r}) e^{-i\vec{Q}\cdot\vec{r}} dV_1 d(V_1 - V)$$

$$= \int V\gamma(\vec{r}) e^{-i\vec{Q}\cdot\vec{r}} d(V_1 - V) = \int V\gamma(\vec{r}) e^{-i\vec{Q}\cdot\vec{r}} dV \qquad V\gamma(\vec{r}) \equiv \int \rho(\vec{r}_1)\rho(\vec{r}_1-\vec{r}) dV_1$$

$$I(Q) = \left\langle A(\vec{Q})\cdot A^*(\vec{Q}) \right\rangle_\Omega = 4\pi \int_0^\infty r^2 V\gamma(r) \frac{\sin Qr}{Qr} dr$$

$$V\gamma(r) \equiv 4\pi \int_0^\infty r_1^2 \rho(r_1)\rho(r_1 - r) dr_1$$

$$I(0) = \int\int \rho(\vec{r}_1)\rho(\vec{r}_2) dV_1 dV_2 = \bar{\rho}^2 V^2$$

$$= 4\pi \int_0^\infty r^2 V\gamma(r) \lim_{Q\to 0} \frac{\sin Qr}{Qr} dr = 4\pi \int_0^\infty r^2 V\gamma(r) dr$$

Analytical scattering intensity of globular particles

$$I(Q) = \left(3\frac{\sin QR - QR\cos QR}{(QR)^3}\right)^2$$

$$p(r) = 12x^2(2 - 3x + x^3) \quad x = r/2R \le 1$$

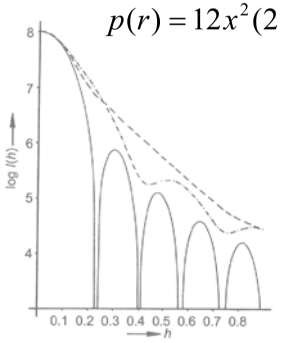

Fig. 2.6.1.5. Comparison of the $I(h)$ functions of a sphere, a prolate, and an oblate ellipsoid (see legend to Fig. 2.6.1.4).

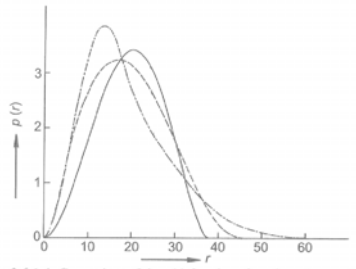

Fig. 2.6.1.4. Comparison of the $p(r)$ function of a sphere (———), a prolate ellipsoid of revolution 1:1:3 (— — —), and an oblate ellipsoid of revolution 1:1:0.2 (- - - -) with the same radius of gyration.

Correlation function

Correlation (characteristic) function (Porod, 1951)

$$V\gamma(r) \equiv 4\pi\int_0^\infty r_1^2\rho(r_1)\rho(r_1 - r)dr_1$$

$$I(Q) = 4\pi\int_0^\infty r^2 V\gamma(r)\frac{\sin Qr}{Qr}dr \qquad V\gamma(r) = \frac{1}{2\pi^2}\int_0^\infty I(Q)Q^2\frac{\sin Qr}{Qr}dQ$$

Porod Invariant $\Delta \equiv 2\pi^2 V\gamma(0) = \int_0^\infty I(Q)Q^2 dQ$ $\qquad V\gamma(0) = 4\pi\int_0^\infty r_1^2\rho^2(r_1)dr_1 = V\overline{\rho}^2$

Correlation length (i.e. mean width of γ(r)) $l_c = \frac{\pi}{\Delta}\int_0^\infty I(Q)QdQ$

Volume of particles $V = 2\pi^2\frac{I(0)}{\Delta}$

Pair-distance distribution function

Pair-distance distribution function (Guiner, 1955)

$$p(r) \equiv r^2 V\gamma(r) \qquad I(Q) = 4\pi\int_0^\infty r^2 V\gamma(r)\frac{\sin Qr}{Qr}dr$$

$$I(Q) = 4\pi\int_0^\infty p(r)\frac{\sin Qr}{Qr}dr \qquad p(r) = \frac{1}{2\pi^2}\int_0^\infty I(Q)Qr\sin QrdQ$$

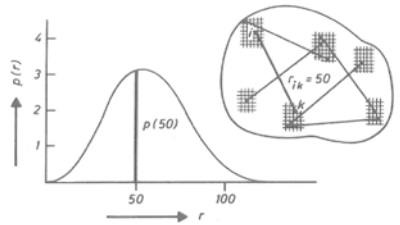

Fig. 2.6.1.1. The height of the $p(r)$ function for a certain value of r is proportional to the number of lines with a length between r and $r + dr$ within the particle.

$$I(0) = 4\pi\int_0^\infty p(r)dr = 4\pi\int_0^\infty r^2 V\gamma(r)dr$$

$$p(50) = 4\pi(50)^2\int_0^\infty r_1^2\rho(r_1)\rho(r_1 - 50)dr_1$$

Guinier Law and Radius of gyration

$$R_g^2 \equiv \frac{\int_V r_i^2\rho(\vec{r}_i)dV_i}{\int_V \rho(\vec{r}_i)dV_i} = \frac{\int_0^\infty r^2 p(r)dr}{2\int_0^\infty p(r)dr}$$

Guinier approximation is applied for the innermost part of the scattering curve.

$$I(Q) = I(0)\exp(-Q^2R_g^2/3) \qquad 0 < QR_g < 1.3$$

Guinier plot of logI(Q) vs Q^2 shows a linear descent with a slope tanα, where

$$R_g^2 = K^2\tan\alpha \qquad \tan\alpha = \frac{\Delta\log I(Q)}{\Delta Q^2}$$

$$K = \sqrt{\frac{3}{\log e}} = 2.628$$

Radius of gyration of simple homogneous bodies

Sphere	$R_g^2 = (3/5)R^2$
Hollow sphere	$R_g^2 = (3/5)\dfrac{R_2^5 - R_1^5}{R_2^3 - R_1^3}$
Ellipsoid	$R_g^2 = (1/5)(a^2 + b^2 + c^2)$
Parallelepiped	$R_g^2 = (1/12)(a^2 + b^2 + c^2)$
Elliptic cylinder	$R_g^2 = \dfrac{a^2 + b^2}{4} + \dfrac{h^2}{12} \equiv R_c^2 + \dfrac{h^2}{12}$
Hollow cylinder	$R_g^2 = \dfrac{R_1^2 + R_2^2}{2} + \dfrac{h^2}{12}$

Radius of gyration of the cross section R_c

For rod-like particles

$$R_c^2 = \frac{\int_0^\infty r^2 p_c(r)dr}{2\int_0^\infty p_c(r)dr} \qquad I_c(Q) \equiv I(Q)Q$$

$$p_c(r) = \frac{1}{2\pi^2}\int_0^\infty I_c(Q)Qr\sin Qr dQ$$

$$I_c(Q) = I_c(0)\exp(-Q^2R_c^2/2)$$

$$R_c^2 = K_c^2 \tan\alpha \qquad \tan\alpha = \frac{\Delta \log I_c(Q)}{\Delta Q^2}$$

$$K_c = \sqrt{\frac{2}{\log e}} = 2.146$$

Cross section $\quad A = 2\pi \dfrac{\lim_{Q\to 0} I_c(Q)}{\Delta}$

Radius of gyration of the thickness R_t

For disc-like particles

$$R_t^2 = \frac{\int_0^\infty r^2 p_t(r)dr}{2\int_0^\infty p_t(r)dr} \qquad I_t(Q) \equiv I(Q)Q^2$$

$$p_t(r) = \frac{1}{2\pi^2}\int_0^\infty I_t(Q)Qr\sin Qr dQ$$

$$I_t(Q) = I_t(0)\exp(-Q^2R_t^2)$$

$$R_t^2 = K_t^2 \tan\alpha \qquad \tan\alpha = \frac{\Delta \log I_t(Q)}{\Delta Q^2}$$

$$K_t = \sqrt{\frac{1}{\log e}} = 1.517$$

Thickness $\quad T = \pi \dfrac{\lim_{Q\to 0} I_t(Q)}{\Delta}$

Absolute intensity and molecular mass

$$I(0)/c \propto M.M.$$

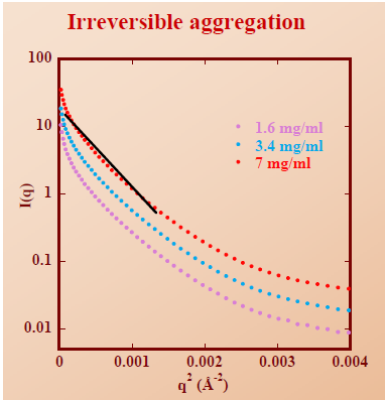

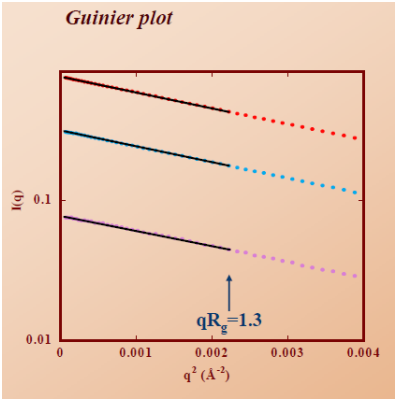

Interaction and 2nd virial coeffience

In the case of intermolecular interactions, I(0)/c is concentration dependant.

$$I(0,c) = \frac{I(0)_{ideal}}{1+2A_2Mc+\ldots} = \frac{Kc}{1+2A_2Mc+\ldots}$$

Porod Law: asymptotic regime

Hypothesis: The particle has a uniform electron density and a sharp interface with the solvent.

$$\lim_{Q\to\infty}[i_1(Q)] = 2\pi S\Delta\rho^2 Q^{-4} + B$$

S is the area of the solute/solvent interface

Kratky plot: $Q^2I(Q)$ vs Q

The degree of compactness
Globular particle: bell-shaped curve (asymptotic behaviour in q^{-4})

Gaussian chain: plateau at large Q (asymptotic behaviour in q^{-2})

$$\lim_{Q\to\infty}[Q^2I(Q)] = \frac{2(1-(QR_g)^{-2})}{R_g^{\ 2}}$$

SAXS

Scattering contrast:

$I_{contrast}(Q) =$ 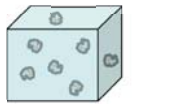 - 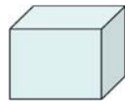

$I_{solution}(Q)$ $I_{solvent}(Q)$

 -  + 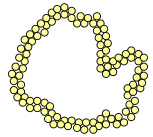

protein excluded solvent bound solvent contrast

$$I_{contrast}(Q) = \left\langle \left| \vec{A}_{protein}(\vec{Q}) - \rho_{solvent}\vec{E}_{excluded\ volume}(\vec{Q}) + \delta\rho_b\vec{B}_{bound\ solvent}(\vec{Q}) \right|^2 \right\rangle_\Omega$$

Scattering length density:

Protein ~ 1.21 x 10^{11} cm^{-2}; Solvent ~ 9.4 x 10^{10} cm^{-2}; Bound solvent ~ 1.14 x 10^{11} cm^{-2}

Spherical Harmonics Approach

$$I(Q) = 2\pi^2 \sum_{l=0}^{\infty} \sum_{m=-l}^{l} \left| \bar{A}_{lm}(\bar{Q}) - \rho_0 \bar{E}_{lm}(\bar{Q}) + \delta\rho_b \bar{B}_{lm}(\bar{Q}) \right|^2$$

$$A_{lm}(Q) = 4\pi i^l \sum_j \left[f_j(Q) \sum_{l=0}^{\infty} \sum_{m=-l}^{l} j_l(Qr) Y_{lm}^*(\theta,\varphi) \right]$$

Form factor of the atomic group:

$$f_j(Q) = \sqrt{\sum_{i=1}^{N} \sum_{k=1}^{N} f_i(Q) f_k(Q) \frac{\sin d_{ik} Q}{d_{ik} Q}}$$

$$Y_{lm}(\theta,\varphi) = \sqrt{\frac{(2l+1)(l-m)!}{4\pi(l+m)!}} P_{lm}(\cos\theta) e^{im\varphi}; \quad P_{lm}(x) = (-1)^m (1-x^2)^{m/2} \frac{d^m}{dx^m}[P_l(x)]; \quad P_l(x) = \frac{1}{2^l l!} \frac{d^l}{dx^l}[(x^2-1)^l]$$

$$P_{00}(\cos\theta) = 1; P_{10}(\cos\theta) = \cos\theta; P_{11}(\cos\theta) = -\sin\theta$$

Spherical Harmonics Approach

$$E_{lm}(Q) = 4\pi i^l \sum_j \left[g_j(Q) \sum_{l=0}^{\infty} \sum_{m=-l}^{l} j_l(Qr) Y_{lm}^*(\theta,\varphi) \right]$$

Form factor of the dummy solvent atoms:

$$g_j(Q) = G(Q) V_j \exp(-\pi Q^2 V_j^{2/3})$$

$$V_j = (4\pi/3) r_j^3$$

$B_{lm}(Q)$ are computed as in shape determination routines.

Angular envelope function:

$$F(\theta,\varphi) = \sum_{l=0}^{\infty} \sum_{m=-l}^{l} f_{lm} Y_{lm}^*(\theta,\varphi)$$

$$\delta\rho_b(\vec{r}) = \begin{cases} 1, & F(\theta,\varphi) \le r < F(\theta,\varphi) + \Delta(0.3nm) \\ 0, & otherwise \end{cases}$$

Crysol: predict solution scattering curve with a pdb

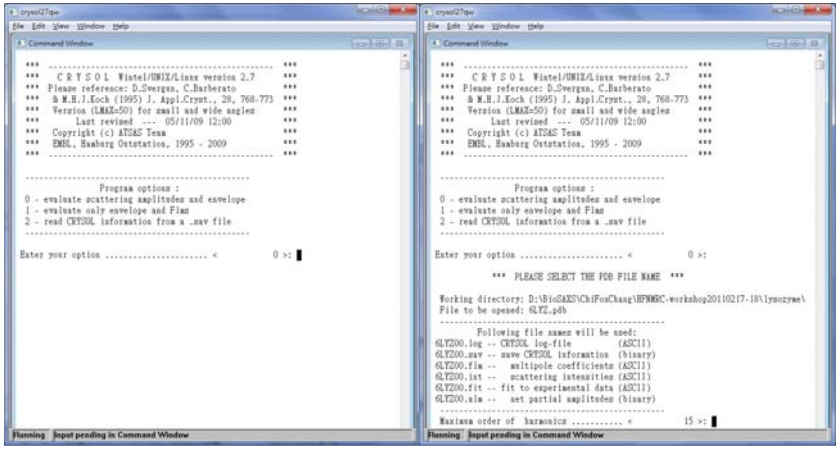

Crysol

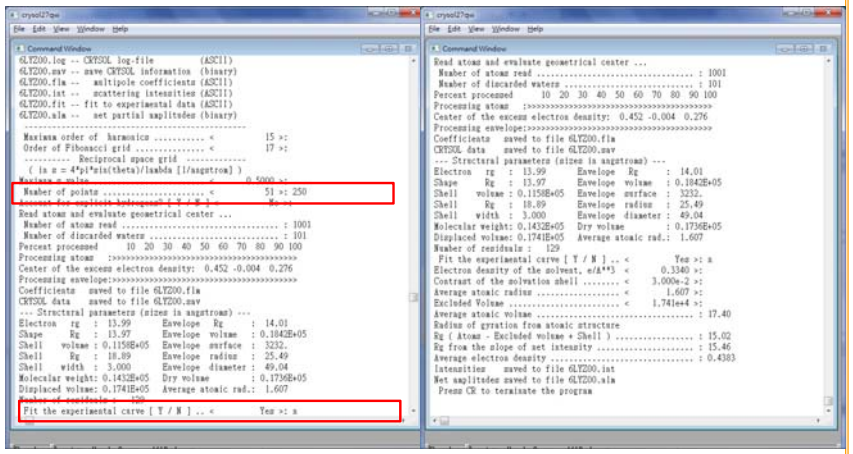

Number of points: 250
Fit exp. Curve: n

CRYSOL—predict solution scattering curve with a pdb

Input : pdb file

Output : *.log → record parameter used in CRYSOL calc. and also final calc. Rg value

*.alm → net partial amplitude

*.int → scattering intensities

```
Dif/Atom/Shape/Bord 6LYZ.PDB      Dro:  0.030 Ra: 1.6073 Rg: 0.00 Vtot:  18424.
 0.000000E+00  0.486252E+07  0.982521E+08  0.338098E+08  0.150094E+06
 0.724638E-02  0.484241E+07  0.580520E+08  0.336950E+08  0.149067E+06
 0.144928E-01  0.478259E+07  0.574563E+08  0.333533E+08  0.146022E+06
 0.217391E-01  0.468445E+07  0.564763E+08  0.327911E+08  0.141070E+06
 0.289855E-01  0.455022E+07  0.551381E+08  0.320193E+08  0.134375E+06
 0.362319E-01  0.438298E+07  0.534465E+08  0.310526E+08  0.126167E+06
 0.434783E-01  0.418647E+07  0.514542E+08  0.299089E+08  0.116723E+06
 0.507246E-01  0.396498E+07  0.491910E+08  0.286093E+08  0.106347E+06
 0.579710E-01  0.372310E+07  0.466976E+08  0.271770E+08  0.953608E+05
 0.652174E-01  0.346603E+07  0.440176E+08  0.256366E+08  0.840896E+05
 0.724638E-01  0.319852E+07  0.411962E+08  0.240141E+08  0.728460E+05
 0.797101E-01  0.292561E+07  0.382787E+08  0.223352E+08  0.619184E+05
 0.869565E-01  0.265204E+07  0.353100E+08  0.206256E+08  0.515592E+05
 0.942029E-01  0.238220E+07  0.323327E+08  0.189097E+08  0.419779E+05
 0.101449E+00  0.212004E+07  0.293670E+08  0.172102E+08  0.333344E+05
 0.108696E+00  0.186900E+07  0.265091E+08  0.155482E+08  0.257373E+05
 0.115942E+00  0.163191E+07  0.237911E+08  0.139420E+08  0.192437E+05
 0.123188E+00  0.141100E+07  0.210804E+08  0.124074E+08  0.138629E+05
 0.130435E+00  0.120788E+07  0.185793E+08  0.109573E+08  0.956088E+04
 0.137681E+00  0.102357E+07  0.162450E+08  0.960159E+07  0.626768E+04
 0.144928E+00  0.858508E+06  0.140897E+08  0.834757E+07  0.388504E+04
 0.152174E+00  0.712642E+06  0.121208E+08  0.719961E+07  0.229496E+04
 0.159420E+00  0.586470E+06  0.103410E+08  0.615957E+07  0.136803E+04
 0.166667E+00  0.476124E+06  0.874924E+07  0.522700E+07  0.971302E+03
 0.173913E+00  0.383651E+06  0.734077E+07  0.439945E+07  0.975179E+03
 0.181159E+00  0.306086E+06  0.610799E+07  0.367276E+07  0.125905E+04
 0.188406E+00  0.242531E+06  0.504089E+07  0.304143E+07  0.171557E+04
 0.195652E+00  0.191219E+06  0.412772E+07  0.249890E+07  0.225350E+04
```

q difference atomic shape border

(protein) (solvent) (bound solvent)

$$I_{difference} = \left| \sqrt{I_{atomic}} - \sqrt{I_{shape}} + \sqrt{I_{border}} \right|^2$$

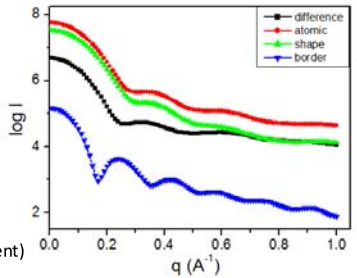

Oligomers

SAXS data of lysozyme (6LYZ) by CRYSOL

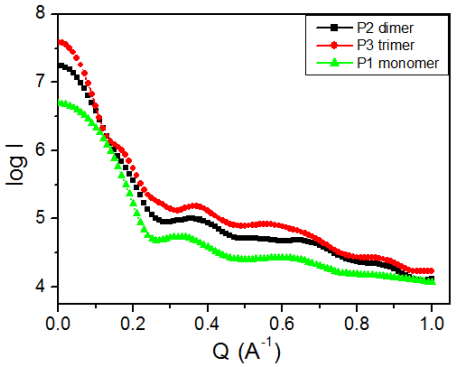

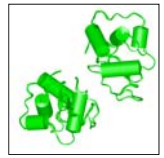

Primus: data reduction and verification

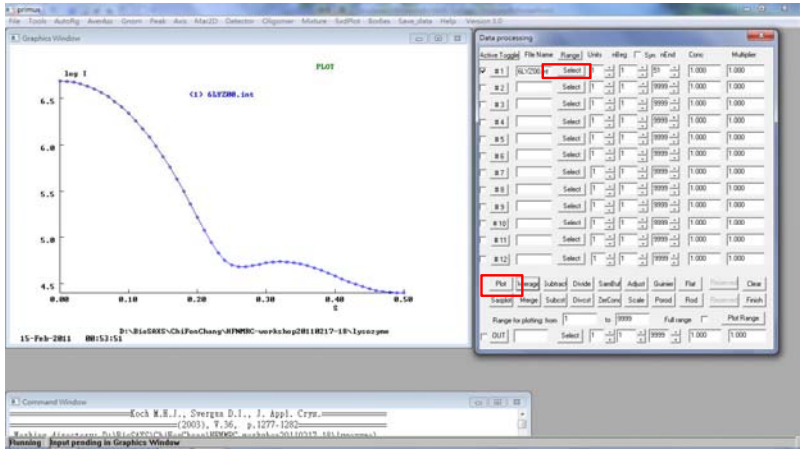

Click “Tool” to open the “data processing” tab

Click select to input your data, click plot to plot your data.

Primus: data reduction and verification

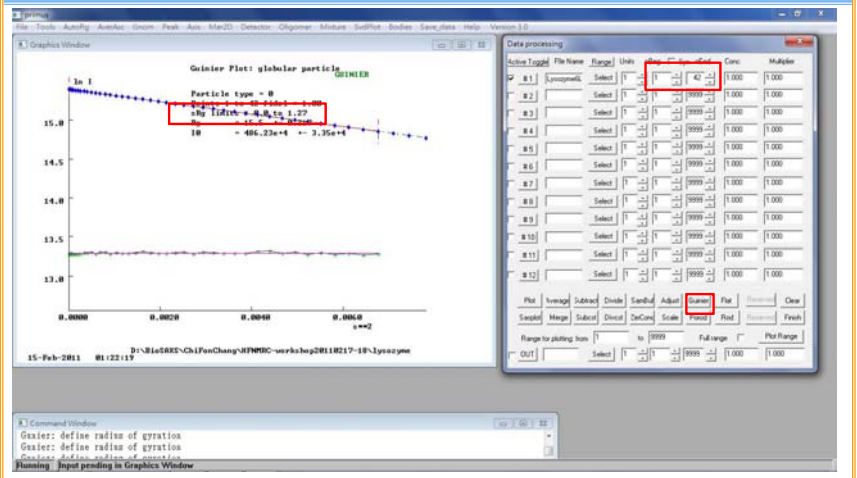

•Click “Guinier” to plot the Guinier plot

•Modify the data range to let sRg <1.3 and chek if the data has good Guinier region

Gnom: P(r)

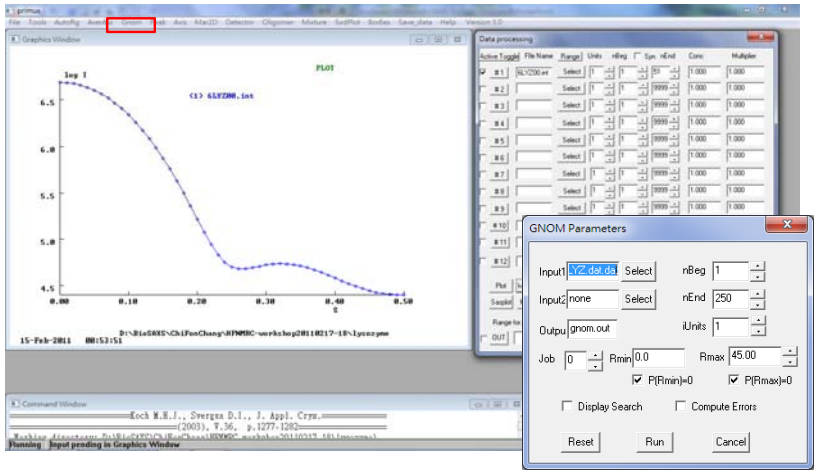

•Click “Gnom” to calculate P(r)
• Set Rmax, Click “Run”

Gnom: P(r)

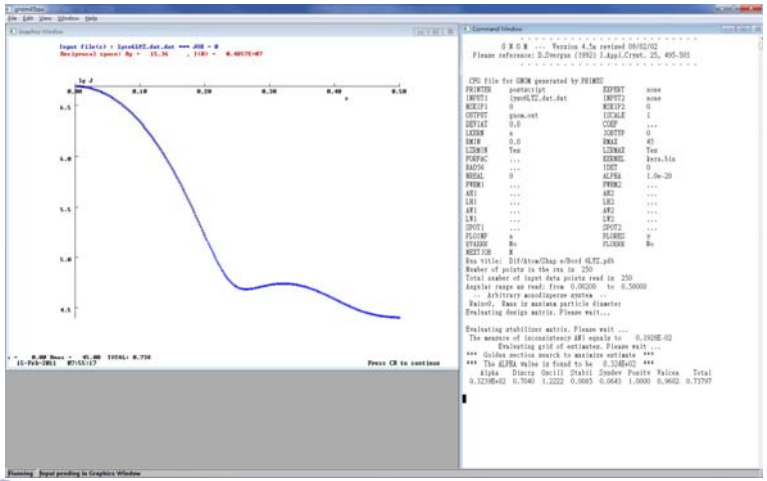

Gnom: P(r)

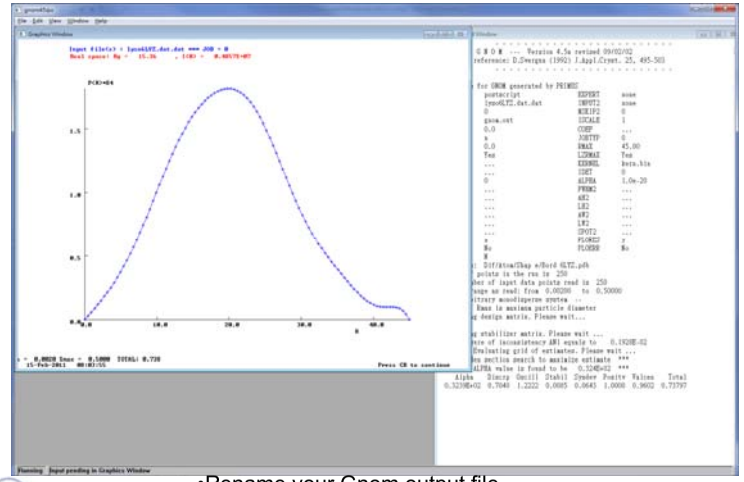

•Rename your Gnom output file

SAXS Reveals Protein Structures

From SAXS analysis by using ATSAS package (Svergun et al), it is possible to:

- **Model the structure evolution of macromolecules during unfolding process (Gasbor, Dammin),**
- **Validate theoretically predicted models (Crysol),**
- **Analyze similarities between macromolecules in solution and in the crystal (Crysol),**
- **Model the quaternary structure of multi-subunit complex by rigid-body refinement against SAXS data (Sasref, Bunch, Monsa).**

Dummy Residue Simulation: Gasbor

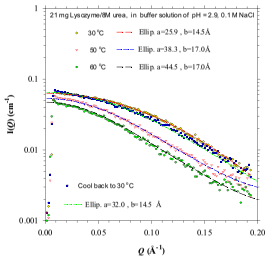

Re-calculate SAXS profile

Gnom

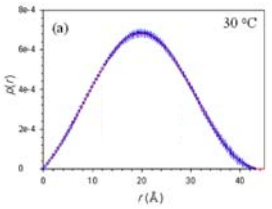

Fit p(r) using **Gasbor** based on ab inition model analysis

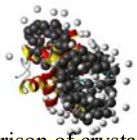

Comparison of crystal structure and solution structure

CRYSOL + modified PDB

Unfolding Process of Lysozyme by Temperature

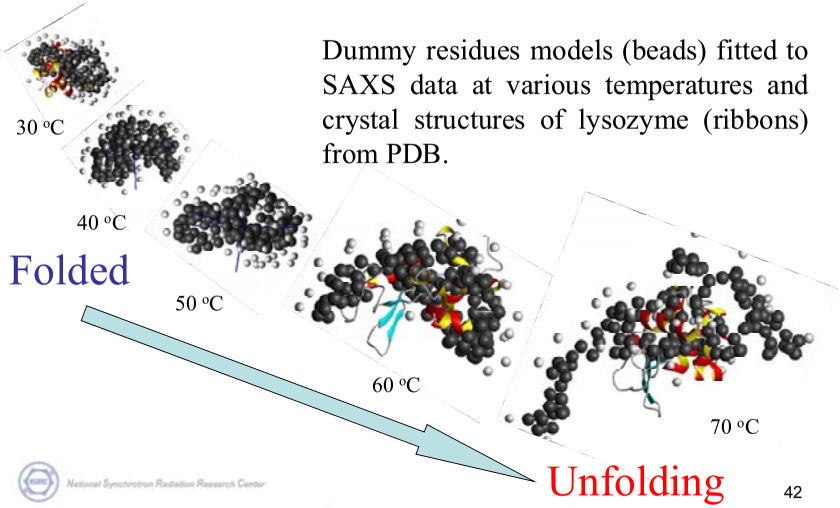

Dummy residues models (beads) fitted to SAXS data at various temperatures and crystal structures of lysozyme (ribbons) from PDB.

Rigid-body Refinement Reveals Quaternary Structure

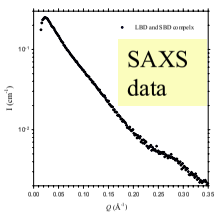

SAXS data

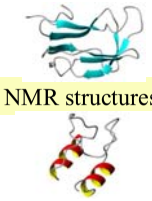

NMR structures

SASREF data fitting

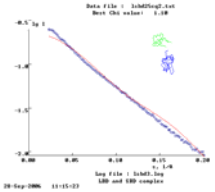

Rigid Body Refinement for an integrated PDB of the two sub-units

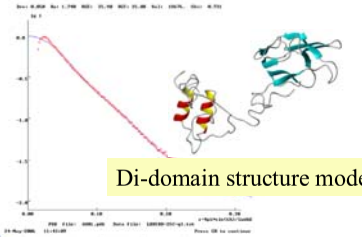

Di-domain structure model